Landslide Processes Involved in Volcano Dismantling From Past to Present: The Remarkable Open-Air Laboratory of the Cirque de Salazie (Reunion Island)

Claire Rault, Yannick Thiery, Marie Chaput, Pierre-Alexandre Reninger, Thomas Dewez, Laurent Michon, Kevin Samyn, Bertrand Aunay

HAL Id: hal-03674815

https://hal.univ-reunion.fr/hal-03674815v1

Submitted on 21 May 2022 (v1), last revised 8 Sep 2022 (v2)

JGR Earth Surface

Landslide Processes Involved in Volcano Dismantling From Past to Present: The Remarkable Open-Air Laboratory of the Cirque de Salazie (Reunion Island)

C. Rault[1] , Y. Thiery[2] , M. Chaput[1] , P. A. Reninger[2] , T. J. B. Dewez[2] , L. Michon[3,4] , K. Samyn[1] , and B. Aunay[1]

[1]BRGM, Saint-Denis, France, [2]BRGM, Orléans, France, [3]Université Paris Cité, Institut de Physique du Globe de Paris, CNRS, UMR 7154, Paris, France, [4]Laboratoire GéoSciences Réunion, Université de La Réunion, Saint-Denis, France

Abstract The Cirque de Salazie is one of the large erosional depressions of Reunion Island. Composed of a thick accumulation of loose volcaniclastic materials derived from successive volcanic flank collapses and exposed to high precipitation rates, this large depression is particularly prone to landslides. Of the 133 km^2 making up this large depression, at least 19% of slopes are affected by various types of landslides. The diversity and high density of landslides is one of the main issues for inhabited areas. We examine the landslides in this area with the goal of providing key elements for better hazard assessment and understanding their role in the landscape's evolution. For over 20 years, we have been acquiring multidisciplinary data on landslides. In this *cirque*, eight types of landslides are identified and described following an adapted landslide classification. Using a multidisciplinary approach, we characterize and interpret the surface morphology and internal structure of three large inhabited compound landslides with volumes of 0.1 km^3 moving up to 1.15 myr^{-1}. These complex landslides provide an opportunity to investigate the influence of past slope movements on current slope movements. Furthermore, using detailed mapping and volume calculation of the landslides triggered by the last major cyclonic rainstorm, we estimate that rainfall-triggered landslides contribute up to 20% of the long-term erosion rate. The Cirque de Salazie is a remarkable laboratory that offers new insights and challenges for future research on landslide hazard assessment and the role of landslides in the short- and long-term dismantling of volcanoes.

Plain Language Summary An exceptional diversity and density of landslides is observed in the Cirque de Salazie (Reunion Island). Whatever their type (slow-moving to sudden landslides), they all cause significant damage to buildings and infrastructure. They also contribute to the dismantling of the island at longer time scales. We have collected multiple types of data on these landslides over 20 years in order to understand their dynamics and eventually improve the related hazard assessment. These data allow us to define and characterize eight landslide types that are all controlled by the hydrometeorological conditions of the *cirque*, making Salazie an ideal laboratory to study the erosion-related interactions.

1. Introduction

Volcanic edifices often exhibit an eventful geological history characterized by constructive and destructive phases (Carracedo et al., 1999; Gayer et al., 2021; Thouret, 1999; Zernack & Procter, 2021). Volcanic terrains are characterized by a combination of specific environmental factors that make them prone to landslides, such as high relief, steep slopes, weathered and fractured materials, alternating layers of lavas and volcaniclastic deposits with different mechanical characteristics, and preferential shear surfaces (Roverato et al., 2015; Scott et al., 2001; Tibaldi et al., 2008). They are also exposed to processes known to trigger failures, such as volcanic activity with hydrothermal circulation, fluid injection, earthquakes (Di Traglia et al., 2018; Roverato et al., 2021; Schaefer et al., 2019) and high precipitation rates, especially in tropical environments.

Volcanic edifices are prone to the full spectrum of landslide sizes ranging from giant debris or rock avalanches (RA) of several km^3 to small rockfalls, including:

1. Large-scale volcanic landslides (e.g., slumps and debris avalanches [DA]) with various magnitudes and kinematics may occur several times during the evolution of a volcano. These landslides can reach volumes of several km^3, which can correspond to the destabilization of an entire volcanic flank (Blahůt et al., 2019;

Project Administration: B. Aunay
Software: C. Rault
Supervision: Y. Thiery, B. Aunay
Validation: C. Rault, M. Chaput
Visualization: C. Rault, Y. Thiery
Writing – original draft: C. Rault, Y. Thiery, M. Chaput, P. A. Reninger
Writing – review & editing: C. Rault, Y. Thiery, M. Chaput, P. A. Reninger, L. Michon, B. Aunay

Carracedo et al., 1999; Holcomb & Searle, 1991; Martí et al., 1997; Masson, 1996; Moore et al., 1989; Oehler et al., 2008; Okubo, 2004; Schaefer et al., 2019; Vallance & Scott, 1997; Voight & Elsworth, 1997; Watt et al., 2014; Zernack & Procter, 2021).

2. Large destabilization phenomena exceeding 10^6 m^3 that mobilize rock or volcaniclastic deposits may move rapidly (e.g., RA and debris flows [DF]) or slowly (e.g., compound slides and rotational slides [RtSs]; Belle et al., 2014; Del Potro & Hürlimann, 2008; McGuire, 1996; Rodrigues & Ayala-Carcedo, 2002; Sibrant et al., 2015; Smith & Lowe, 1991; Valadão et al., 2002).

3. Smaller landslides mobilizing volumes less than 10^6 km^3 frequently occur on steep slopes, such as steep valleys and caldera/crater walls (Barbano et al., 2014; Di Martire et al., 2012; Dou et al., 2019; Ferrucci et al., 2005; Hibert et al., 2011; McGuire, 1996; Selva et al., 2019; Tommasi et al., 2005; Valadão et al., 2002).

These processes produce a succession of volcaniclastic deposits available for erosion and landslide processes (Major et al., 2005; Rossignol et al., 2019; Zanchetta et al., 2004; Zernack, 2021). While the major landslide events during the main degradation phases are widely studied with different hypotheses on dismantling (Roverato et al., 2021), smaller-scale remobilization processes of volcaniclastic deposits by landslides are less understood (Bernard et al., 2009). Understanding the involvement of landslides in the destruction of the volcanic edifice is of prime importance for hazard assessment in inhabited volcanic areas (Calcaterra et al., 2007). One way to improve knowledge is to recognize, describe and delineate the variety of landslides (type of movement, material involved, kinematics, frequency of occurrence, and forcings) occurring in such environments and then to quantify their role in dismantling.

Salazie, the westernmost *cirque* of Reunion Island, provides a good location for such a study. Reunion is a tropical island with young, high reliefs shaped by a high erosion rate, mainly due to slope failure processes (Bret et al., 2003; Gayer et al., 2019; Haurie, 1987; Holcomb & Searle, 1991; Humbert et al., 1981; Karátson et al., 1999; Louvat & Allègre, 1997; Oehler et al., 2008). The three largest and deepest depressions (Salazie, Mafate, and Cilaos), called *cirques*, are located in the center of the island. They are the result of the dismantling of the Piton des Neiges (PN) volcanic edifice. They have been eroded during the last period of quiescence of the edifice; that is, since ~70 ka (Bret et al., 2003; Gayer et al., 2019; Salvany et al., 2012). These depressions are filled with volcaniclastic deposits that are particularly prone to erosion and landslides. The Cirque de Salazie contains a variety of both rapid landslides (velocity $>5 \times 10^{-1}$ mm s^{-1}; Cruden & Varnes, 1996) and large slow-moving landslides (volume > 0.1 km^3) (Belle et al., 2014; Haurie, 1987; Humbert et al., 1981; Pinchinot, 1984), offering the opportunity to study the different landslide processes involved in the remobilization of ancient volcaniclastic deposits.

This study proposes to define the different types of landslides involved in the dismantling of the edifice in the recent past and present-day. Our multidisciplinary approach combines:

1. Classical approaches such as field observations, morphological analyses on digital terrain models, analyses of the velocities of some landslides through assessments of old differential global positioning system monitoring and new acquisitions by the same type of device and a reinterpretation of old reports and previous data (e.g., the diachronic analysis of aerial photographs) obtained over the last 40 years;

2. Innovative methods such as the analysis of soil and subsoil data from a heliborne electromagnetic survey (AEM; Nakazato & Konishi, 2005; Reninger et al., 2020) and the analysis of ground velocities and deformations through a lidar approach (digital elevation model [DEM] of difference and 3D point cloud comparison) (James et al., 2012; Stumpf et al., 2015).

In this paper, we propose new insights into the current and past dynamics of the dismantling of a volcanic edifice by landslides with volumes of less than 1 km^3 through (a) the identification and classification of landslides based on morphology and involved materials, (b) the conceptualization of their mechanisms and their kinematic behaviors, (c) the understanding of their role in erosion processes and landscape evolution, and (d) their implications for landslide hazard assessment.
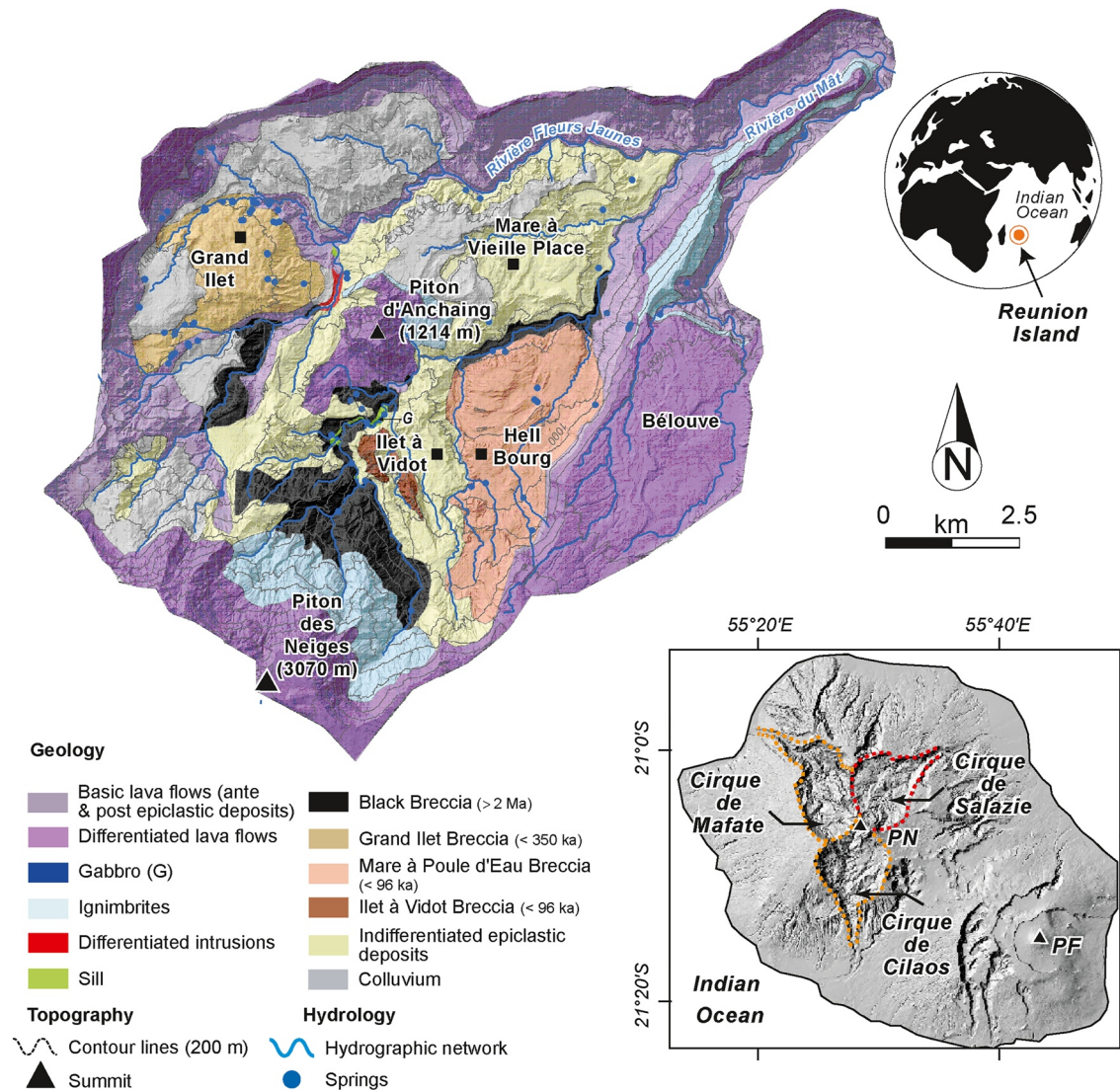
Figure 1. Geology of the Cirque de Salazie. Fifty-five percent of the surface of the *cirque* is covered by volcaniclastic material (breccia units and colluvium) resulting from the progressive dismantling of the Piton des Neiges (PN) edifice (Arnaud, 2005; Chaput, 2013; Lacquement & Nehlig, 2008; Salvany et al., 2012) (map adapted from Michon (2017)). Piton d'Anchaing is a megablock coming from a large slope movement whose type is still debated (Arnaud, 2005; Famin et al., 2016; Haurie, 1987). The main villages of Salazie are indicated by black squares. The inset at the bottom right of the figure shows the topographic map of Reunion Island, the location of the PN and Piton de la Fournaise volcanoes, and the position of the three *cirques* surrounded by dotted lines, with the Cirque de Salazie contoured in red.

2. Study Site

2.1. Reunion Island

Reunion Island is a small volcanic island (2,512 km²; Figure 1) located in the southwest Indian Ocean approximately 300 km north of the Tropic of Capricorn (21°S and 55°E). The island is formed of two volcanoes, the active Piton de la Fournaise to the east and the dormant PN to the west, culminating at 3,070 m above sea level (a.s.l.). Three large depressions called *cirques* radiate from the summit of PN: the Cirque de Salazie to the north, the Cirque de Mafate to the west, and the Cirque de Cilaos to the south (Figure 1). The *cirques* are enlarged valleys that are very dissected and narrow toward the sea (Cilaos is almost circular, Mafate triangular, and Salazie has a funnel-shaped morphology). These depressions have been interpreted as scars of large flank collapses (Oehler et al., 2004, 2008), as "leaf grabens" caused by gravitational spreading (Borgia et al., 2000; Byrne et al., 2013; Delcamp et al., 2008, 2012), as a consequence of plutonic complex subsidence (Gailler & Lénat, 2012) or as purely regressive erosional structures (Gayer et al., 2019; Haurie, 1987; Salvany et al., 2012).
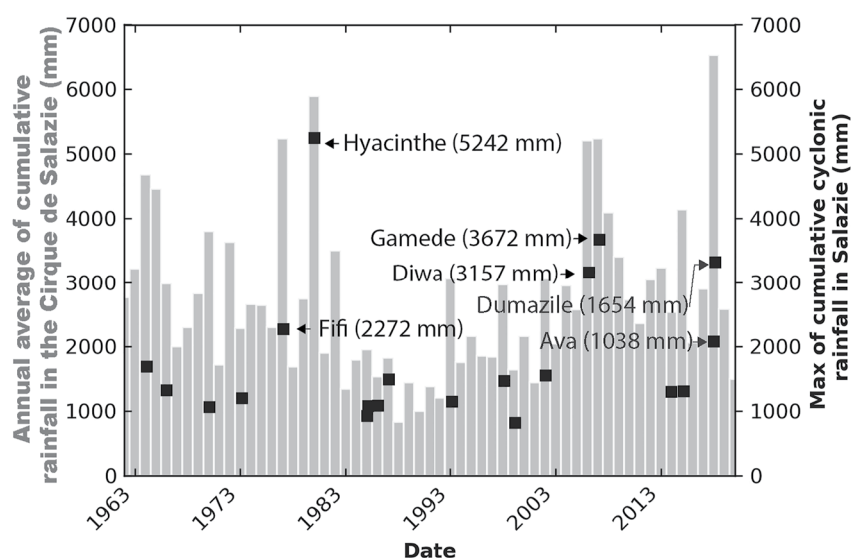
Figure 2. Annual average cumulative rainfall over the Cirque de Salazie since 1962 (for the rainfall average of the Grand Ilet, Salazie and Ilet à Vidot stations, see Figure S3 in Supporting Information S1). The mean annual rainfall in Salazie is approximately 2,500 mm. The black squares indicate the maximum cumulative rainfall recorded in Salazie during extreme events (cumulative rainfall >500 mm). The names of four of the major cyclones and their cumulative rainfall recorded in Salazie are given. Since 1964, the rainfall accumulated during extreme events has varied from approximately 600 mm to 5,242 mm. No precise rainfall data are available for the *cirque* before 1964, especially for extreme events (cf., http://www.meteofrance.re/climat/pluies-annuelles).

The island is regularly hit by tropical cyclones (TCs), which develop over the southwest Indian Ocean (approximately 10 TCs form in this region every year, cf., http://www.meteofrance.re/cyclone/saisons-passees). The strong orographic effect of the island influences the intensity and track of cyclones, which are apt to trigger heavy rainfall (Barbary et al., 2019; Pohl et al., 2016). As a result, Reunion Island holds world records for amounts of intense rainfall (e.g., 1,825 mm in 24 hr during TC Denise in 1966, 5,678 mm in 10 days and 6,083 mm in 15 days during TC Hyacinthe in 1980) (Barcelo et al., 1997; Chaggar, 1984; Quetelard et al., 2009). The windward coast of the island, that is, the northeast coast, is particularly wet due to the trade wind regime and the orographic effect (Barcelo & Coudray, 1996; Réchou et al., 2019).

2.2. The Cirque de Salazie

2.2.1. Climatic and Geological Background of the Cirque de Salazie

The Cirque de Salazie is located in the northeast of the island. It covers an area of approximately 133 km² delineated by cliffs over 500 m high (Figure 1). Salazie is the rainiest *cirque* on Reunion Island (e.g., Pohl et al., 2016) with an average annual cumulative rainfall of approximately 3,100 mm since 1963; a minimum of 698 mm was recorded in 1990, and a maximum of 5,893 mm was recorded in 1980 (Figure 2). Heavy rainfalls in Salazie are caused by the advection mechanism and strong orographic uplift (Pohl et al., 2016) favored by the *cirque*'s topography and its geographical position (windward side of the island). Rainfall totals are maximized during cyclonic events. Since 1980, maximum rainfall quantities in Salazie have been recorded during TC Hyacinthe (1980, 5,242 mm), TC Gamède (2007, 3,672 mm), and TC Diwa (2006, 3,157 mm) (Figure 2).

The scarps of the *cirque* are made of a thick basic lava flow sequence capped by differentiated lavas and pyroclastic deposits (ignimbrites) and crosscut in some places by basaltic or differentiated intrusions (dikes or sills; Chaput et al., 2017; Salvany et al., 2012).

Large volumes of volcaniclastic deposits produced and emplaced by epiclastic processes (Suthren, 1985) fill the *cirque*, sometimes with a thickness of 100 m. They comprise several lithological units with weaker rock strength than the lava flow units.

River erosion has incised deep valleys and produced several isolated plateaus across the *cirque*: these are known as *îlets,* and are the most populated areas (Figure S1 in Supporting Information S1). The steep slopes surrounding the *îlets* are incised by numerous gullies, creating a badland morphology.

The environmental conditions favor material weathering and dismantling by erosion processes. Consequently, the morphology of the Cirque de Salazie is constantly evolving (Dupond, 1984; Gayer et al., 2019; Humbert et al., 1981; Karátson et al., 1999). Gayer et al. (2019) estimated that the *cirque* results from a long-term erosion rate of 7.4 ± 0.7 mm yr^{-1} over 72 ka.

2.2.2. Epiclastic Deposits

The largest volumes of volcaniclastic material in the *cirque* have been interpreted as volcanic debris-avalanche deposits or as debris-flow/mud-flow deposits (Arnaud, 2005; Bret et al., 2003; Famin & Michon, 2010; Haurie, 1987; Lacquement & Nehlig, 2008; Michon, 2017; Oehler et al., 2005; Salvany et al., 2012). The term "epiclastic," which reflects their origins, can be used to describe them (e.g., Bernard et al., 2021, 2009; Cas & Wright, 1988; Colmenero et al., 2012; Crosta et al., 2005; Suthren, 1985). The epiclastic deposits in the *cirques* of Reunion Island record large dismantling events of the flanks of PN, from its shield-building stage to the present day.

The observed epiclastic deposits from DA are composed of nongraded, poorly sorted clasts that range in size from centimeters to several meters and comprise various lithologies (volcanic rocks, lava flows, intrusions, volcaniclastic, plutonic rocks, etc.) (Arnaud, 2005; Lacquement & Nehlig, 2008; Perinotto et al., 2015). These deposits frequently present typical volcanic debris-avalanche sedimentary features such as jigsaw cracks, megablocks, and shattered clasts (Arnaud, 2005; Dufresne et al., 2016; Glicken, 1991). They form a characteristic irregular topography exhibiting longitudinal and transverse ridges (Oehler et al., 2004). In some places, these deposits are cross-cut by shear planes inherited from the emplacement of the DA, by postdepositional volcanic-intrusions and/or by fault and shear planes that formed during postdepositional deformations or current movements. In the Cirque de Salazie, at least four different debris-avalanche units are identified: the Black Breccia, the Grand Ilet Breccia, Mare à Poule d'Eau Breccia and the Ilet à Vidot Breccia (Figure 1; Chaput, 2013; Lacquement & Nehlig, 2008; Oehler et al., 2008; Perinotto, 2014).

The Black Breccia is characterized by a clast-supported gravel facies with an irregular clay matrix (Arnaud, 2005). This unit results from flank failures of the edifice during its early stage of activity (>2 Ma; Berthod et al., 2016), with propagation toward the north (Berthod et al., 2016; Chaput, 2013; Famin & Michon, 2010; Famin et al., 2016).

Grand Ilet Breccia is a thick unit composed of a matrix facies and a clast-supported block facies. The block facies dominates the inner part of the deposit. This facies is composed of pluri-decametric to pluri-metric blocks of lava flows, which are fractured and crushed into jigsaw cracks. The matrix facies is observed along surficial outcrops. The matrix facies is an unsorted and unstratified deposit composed of infra-metric clasts (Arnaud, 2005; Lacquement & Nehlig, 2008).

Mare à Poule d'eau Breccia also forms a thick unit, with a clast-supported block facies. The block facies is composed of pluri-decametric to pluri-metric megablocks preserved within a silty to sandy matrix and mixed facies (Figure S2 in Supporting Information S1). Some of the megablocks have a preserved stratigraphy of lava flows, which often show jigsaw cracks (Arnaud, 2005; Oehler et al., 2005).

Ilet à Vidot Breccia unit has two dominated facies: a block facies and a mixed facies. The mixed facies is a poorly sorted unit composed of angular gravel within a sandy to clay matrix (Arnaud, 2005). The block facies is composed of pluri-decametric blocks with some jigsaw-cracked megablocks (Figure S2 in Supporting Information S1).

These three units are younger than the Black Breccia and were probably emplaced toward the north or the northeast after 350 ka for Grand Ilet (Chaput, 2013) and after 96 ka for Ilet à Vidot and Hell Bourg (Arnaud, 2005).

These debris-avalanche deposits are frequently covered by colluvium resulting from *cirque* cliff collapses or reworking processes of older epiclastic deposits (Arnaud, 2005; Bret et al., 2003; Lacquement & Nehlig, 2008; Salvany et al., 2012).
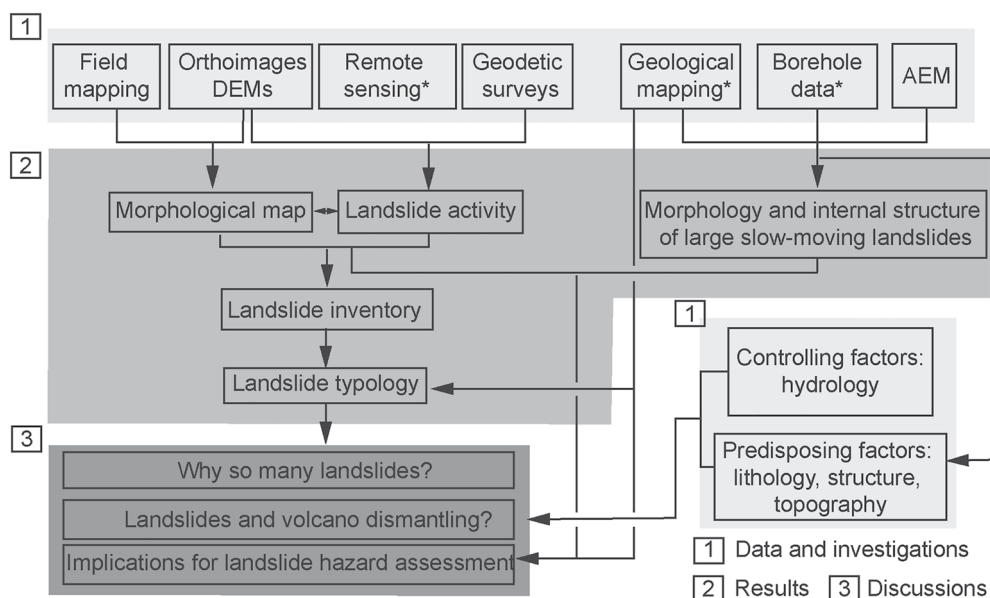
Figure 3. Method flow chart showing the data and investigations used for (1) identifying and describing the different landslide types observed in Salazie, and (2) characterizing the morphology and the internal structure of large landslides. These results and the study on controlling and predisposing factors enable a discussion of (3) the reasons for the density and diversity of landslides in this particular environment, their implications for the dismantling of a volcanic edifice, and the hazards they represent. *Methods exclusively used in previous studies (cf., Table S1 in Supporting Information S1). AEM: heliborne electromagnetic survey; DEM: digital elevation model.

3. Data and Methods

To conduct this study, several complementary methods and observations were used. Figure 3 illustrates the different steps and the applied techniques.

3.1. Geomorphology Mapping and Landslide Inventory

Although previous studies identified large slow-moving landslides, past catastrophic movements and areas with ancient stabilized landslides in the Cirque de Salazie (e.g., Belle et al., 2014; Haurie, 1987; Humbert et al., 1981; see Table S1 in Supporting Information S1), there are still gaps in understanding their spatial extent, sedimentary characteristics and activity.

To compile a more complete landslide inventory, we focused on the landform characteristics of landslides across the *cirque*. We evaluated five indexed morphologic pieces of evidence: (a) main and secondary scarps, (b) depressions, (c) lobes and areas of material accumulation, (d) open cracks and fissures, and (e) vegetation (Dikau et al., 1996; Mather et al., 2003; McCalpin, 1984; Nichol et al., 2006) and their relationship to landslide activity (e.g., Parise & Guzzi, 1992; Turner & Schuster, 1996; Wieczorek, 1984). The fresher and more visible the morphologic indices are, the more recent and more active the processes are (Flageollet, 1996).

We mapped and assessed landslide information from field analysis of surface morphology, analysis of topographic data (50 cm DEM), aerial photographs (from 1950 to 2011) and ortho-images (1997–2017) including information from previous studies (see Table S1 in Supporting Information S1 for more information). Furthermore, the positions of 93 geodetic markers distributed over the *cirque* have been measured regularly since 2003, allowing for the identification of stable and moving areas. Combining this information, we delineated large areas ranging from 100 m^2 to 2.5 km^2 with active and inactive landslides, and mapped documented catastrophic landslides.

To quantify the geomorphic impact of cyclones, we assessed the landslides triggered by Cyclone Hyacinthe (1980), which is considered to be a 100-year rainstorm (Humbert et al., 1981). This cyclone is the most damaging tropical rainstorm for which pre- and post-event aerial photographs are available. We used historical aerial photographs of the *cirque* to build historical digital surface models (DSMs) and orthophotographs using structure from

motion and multiview stereo (SFM-MVS) methods (Gomez et al., 2015; Rault et al., 2020; Riquelme et al., 2019) to map the landslides triggered by the exceptional rainfall associated with TC Hyacinthe and quantify the volume of the mobilized material. For this purpose, the following steps were carried out:

1. Creation of comparable pre- and post-cyclone high-resolution DSMs and orthophotos with available sets of approximately 1:27,000 aerial photographs from 1978, that is, before TC Hyacinthe and from 1984, that is, after TC Hyacinthe, using an SFM-MVS method (Gomez et al., 2015; Rault et al., 2020; Riquelme et al., 2019). The scanned photographs have a resolution of approximately 20 µm per pixel (scanned at 900 dpi). The obtained DSM and the orthophotos have a resolution of 5 and 1 m respectively.

2. Identification and mapping of the landslides between 1978 and 1984, avoiding landslide amalgamation as advised by Marc and Hovius (2015). The mapping procedure involved visual interpretation of pre- and post-cyclonic images, that is, aerial photos, orthophotographs and DSM from 1978 to 1984 (Tanyaş et al., 2017). However, no landslides could be mapped in shaded areas or areas covered by clouds, where changes could not be observed. Additional information on this inventory is provided in Text S1, Figure S4 and Table S2 in Supporting Information S1.

3. Estimation of the volume mobilized by these landslides using the 1978–1984 DSM of difference (DoD; James et al., 2012). The error was assessed by using the difference in elevation for a given slope angle in a stable area that did not show major morphological changes between 1978 and 1984. For each landslide, its volume error is equal to the surface of the landslide multiplied by the mean elevation error given for the landslide slope average. The total error is equal to the sum of the landslide volume errors (see Figure S5 in Supporting Information S1).

3.2. Landslide Typology

The failure mechanisms of landslides involving epiclastic materials are complex and difficult to associate with the classic landslide classifications due to deposit heterogeneities (Hungr et al., 2014).

Thus, we adapted classification criteria and terminology from current landslide classification systems to define a consistent classification for slope failures occurring in the Cirque de Salazie. Table 1 describes the 10 criteria we used to classify and describe the landslides observed in Salazie.

3.3. Characterization of Large Slow-Moving Landslides

3.3.1. Morphology and Internal Structure

The geomorphological map of large landslides was developed using landslide characteristics from field evidence, aerial images, and high-resolution DEM analysis (see Table S1 in Supporting Information S1).

To image the internal structure of large landslides, we used AEM data acquired in 2014 (SkyTEM survey; Sørensen & Auken, 2004) conducted over Reunion Island (Dumont et al., 2019; Martelet et al., 2014). Resistivity contrasts, revealed by this technique, enabled the delineation of interfaces (e.g., weathered or clay layers, faults, and slip surfaces) within shallow and deep landslides (Godio & Bottino, 2001; Nakazato & Konishi, 2005; Thiery et al., 2017, 2021). The resistivity gradient may also be attributed to water circulation (Vittecoq et al., 2019).

The flight lines of this survey were mainly oriented north-south with a 400-m spacing and were more concentrated over areas of particular interest, such as the Cirque de Salazie (Martelet et al., 2014). Several lines extending over the large landslides of Salazie allow these landslides to be imaged laterally and vertically (Figure S6 in Supporting Information S1).

The AEM data were acquired using a low magnetic moment (3,100 Am^2–325 Hz) for near-surface resolution, and a high-magnetic moment (160,000 A m^2–25 Hz) for depth investigation and processed according to Reninger et al. (2011, 2020). One-dimensional AEM soundings showing resistivity variations with depth were achieved, applying a quasi-3D spatially constrained inversion to the remaining AEM data (Viezzoli et al., 2008). Continuous pseudo-3D resistivity models over the large landslides were then obtained by interpolating the 1D AEM soundings. The investigation depth of the method varied locally, depending on the acquisition parameters (emitted magnetic moment and bandwidth used), the signal-to-noise ratio and the surface conductivity.

Table 1
Definition of Criteria Used for the Landslide Typology

Descriptive parameter	Definition
Type of movement	The type of movement describes the kinematics of the landslide. In Salazie two main types of movement can be distinguished: slide and flow
	Slides are a downslope movement of a mass occurring on a failure surface or on a thin layer of intense shear strain (Cruden & Varnes, 1996)
	Flows are spatially continuous movement. Shear surfaces are short-lived and usually not preserved and the material behaves like a viscous fluid during downslope transport (Cruden & Varnes, 1996; Hungr et al., 2001)
Materials	The material contained in a landslide. It allows clearer determination of the mechanical behavior of the landslide (failure and transportation) (Hungr et al., 2014). In Salazie it can be rock or debris (from old epiclastic deposits)
Area	Area impacted by the landslide, including the area of initiation and propagation. For historic rapid landslides, the downstream part of the landslide may have been removed by rivers prior to being photographed, thus the calculated areas of these landslides are minimum estimates
Volume	Volume of the displaced mass. The volume is estimated from geophysical investigations for the largest landslides, and from DEM of difference for the smallest ones
Depth of failure	Depth of failure surface estimated from geophysical investigation or field observations
Topographic slope	Average topographic slope on which the landslide occurs. The topographic slope is determined from DEM analysis
H/L	The ratio between the height of fall (*H*) and the run-out distance (*L*). *H/L* characterizes the landslide mobility (Crosta et al., 2005; Hungr et al., 2001; Legros, 2002). For historical landslides the run-out distance is a minimum estimate, because the downstream part of the landslide may have been removed by rivers prior to being photographed
Water content	The water content of landslide materials defined by observations of the displaced material or inferred from rainfall amounts. The water content is defined as:
	• *Unsaturated:* the moving material contains some water but no free water
	• *Partially saturated:* some of the moving material is saturated, or contains enough water to behave in part as a liquid
	• *Saturated:* the material contains a lot of water and is able to flow
Water forcings	The role of groundwater or surface water in initiating the landslide
Displacement rate	Landslide displacement velocities are classified according to the definition given by Cruden and Varnes (1996). The velocity is estimated from geodetic measurements or estimated from the failure description

To draw a schematic profile of the structures of the landslides, AEM profiles were compared to landslide morphology and geological and structural characteristics from previous geological investigations (Chaput, 2013; Chaput et al., 2014; Famin et al., 2016; Haurie, 1987; Lacquement & Nehlig, 2008; Pinchinot, 1984). In Grand Ilet, these data were also compared to electrical resistivity profiles and borehole data already analyzed (Baltassat et al., 2016; Belle, 2014).

3.3.2. Survey of the Activity of Slow-Moving Landslides

In addition to the geodetic markers, the displacements of the most active landslides are being monitored using eight global navigation satellite system (GNSS) antennas with daily recordings and centimeter precision (Bellanger & Aunay, 2008; Mazué et al., 2013) (Figure S3 in Supporting Information S1). Furthermore, to specify the local variation in the amplitude and direction of displacements, geodetic transect surveys with a 200-m measurement step were carried out before and after the cyclone season in 2012–2013 (Mazué et al., 2013) and 2019–2020.

To explore the relationship between landslide dynamics, pluviometric variations and groundwater circulation, we used:

1. Daily rainfall recorded in the villages of Grand Ilet and Hell Bourg by Météo-France stations. Both stations ensure that the pluviometric data collected on the two landslides is representative due to the low spatial

variability of precipitation at landslide scale. Joint analysis of rainfall and landslide-displacement records aims at establishing empirical relationships amongst time series and identifying potential meteorological thresholds.

2. Maps of springs and closed depressions corresponding to outlets and potential preferential zones of infiltration, respectively (Belle, 2014; Moulin & Lebon, 2002). A potential relation between their locations and landslide structure and/or activity could reflect the influence of groundwater on landslide activity.

4. Results

4.1. Landslide Activity and Movement Rates

More than 1,700 landslides were recognized and mapped in Salazie, and more than 80% of these were added by this study. The mapped landslides cover 19.2% of the total surface of the *cirque* (Figure 5a). Among them, two states of activity can be distinguished: active and inactive (Figure 4). Recently active phenomena make up 94.4% of the mapped landslides, and inactive phenomena represent 5.6% (Figure 5b).

4.1.1. Active Landslides

Active landslides in Salazie have typical morphological features of movement identified on field aerial photographs and DEMs. Among the active landslides, we distinguished slow-moving and rapid landslides.

4.1.1.1. Slow-Moving Landslides

Slow-moving landslides are commonly observed on *îlets*. Seven large slow-moving landslides have been identified in the *cirque* (Grand Ilet, Hell Bourg, Ilet à Vidot, Mathurin, Camp Pierrot Bélier, Mare à Goyaves) (Figure 4 and Figure S7 in Supporting Information S1). Their displacement rates range from a few cm yr^{-1} up to 1.15 m yr^{-1} and accelerate after intense rainfall events (Belle et al., 2014), and they cover areas that vary from tens of thousands of m^2 to several km^2 (see Section 4.3). Their main characteristics are given in Table 2. Slow-moving landslides induce slow and continuous damage to buildings and infrastructures (e.g., cracks and collapses, see Figure S8 in Supporting Information S1).

4.1.1.2. Rapid Landslides: Example of the Landslides Triggered by Cyclone Hyacinthe

Rapid landslides are mostly triggered by intense rainfall and are regularly remobilized during rainfall episodes. These landslides affect the steep slopes of all geomorphological units of the *cirque* (scarps, *îlets*, valleys, and isolated rocky peaks), although most of them are observed on valleys and *îlets* (Figure 4). The 100-year rainstorms associated with Cyclone Hyacinthe (1980) caused a significant amount of destabilization. By comparing the 1978 and 1984 images of the *cirque*, we identified and mapped more than 1,400 landslides that are considered to have been triggered by TC Hyacinthe. Their surface areas vary from 5 m^2 to approximately 2×10^5 m^2 (Figure 6). The probability density function of the landslide surface area (scarp and run-out) for surface areas above 3,000 m^2 displays a power law relationship with an exponent of 2.24 (Figure 6), which is in the range of landslides triggered in mixed soil and rock (Larsen et al., 2010). The estimated volume removed from the slopes by the 1,429 landslides varies from 100 ± 31 to $555 \pm 8.1 \times 10^3$ m^3. The volume-area relationship can be fitted with a power law with an exponent of 1.35. The total volume eroded in the *cirque* from these landslides was estimated by adding the contribution of each landslide with the DoD, and equals approximately $15.2 \pm 0.44 \times 10^6$ m^3.

4.1.2. Inactive Landslides

Landslides that show no recent evidence of erosion or movement were classified as inactive. They are less distinctive, especially in the field (Dikau et al., 1996; Mather et al., 2003). In theory, they can re-activate randomly with return periods ranging from thousands of years to a few decades (Flageollet, 1996). In this study, we classified inactive landslides as not exhibiting evidence of recent movement (i.e., for decades), either in aerial photographs or field observations.

In Salazie, inactive landslides identified from the literature and high-resolution DEM analysis cover 8.2% of the *cirque* area (Figure 5). Les Ramiers (3.39×10^4 m^2; Haurie, 1987) and Grand Sable (9.62×10^5 m^2; Lustremant, 1981) are two examples of inactive landslides, while the Mare à Vieille Place (4.01 km^2) is considered to be a stabilized complex landslide (Haurie, 1987). Its preserved morphology is typical of complex landslides (multiple curved scarps, ponds, counterslopes, etc.).
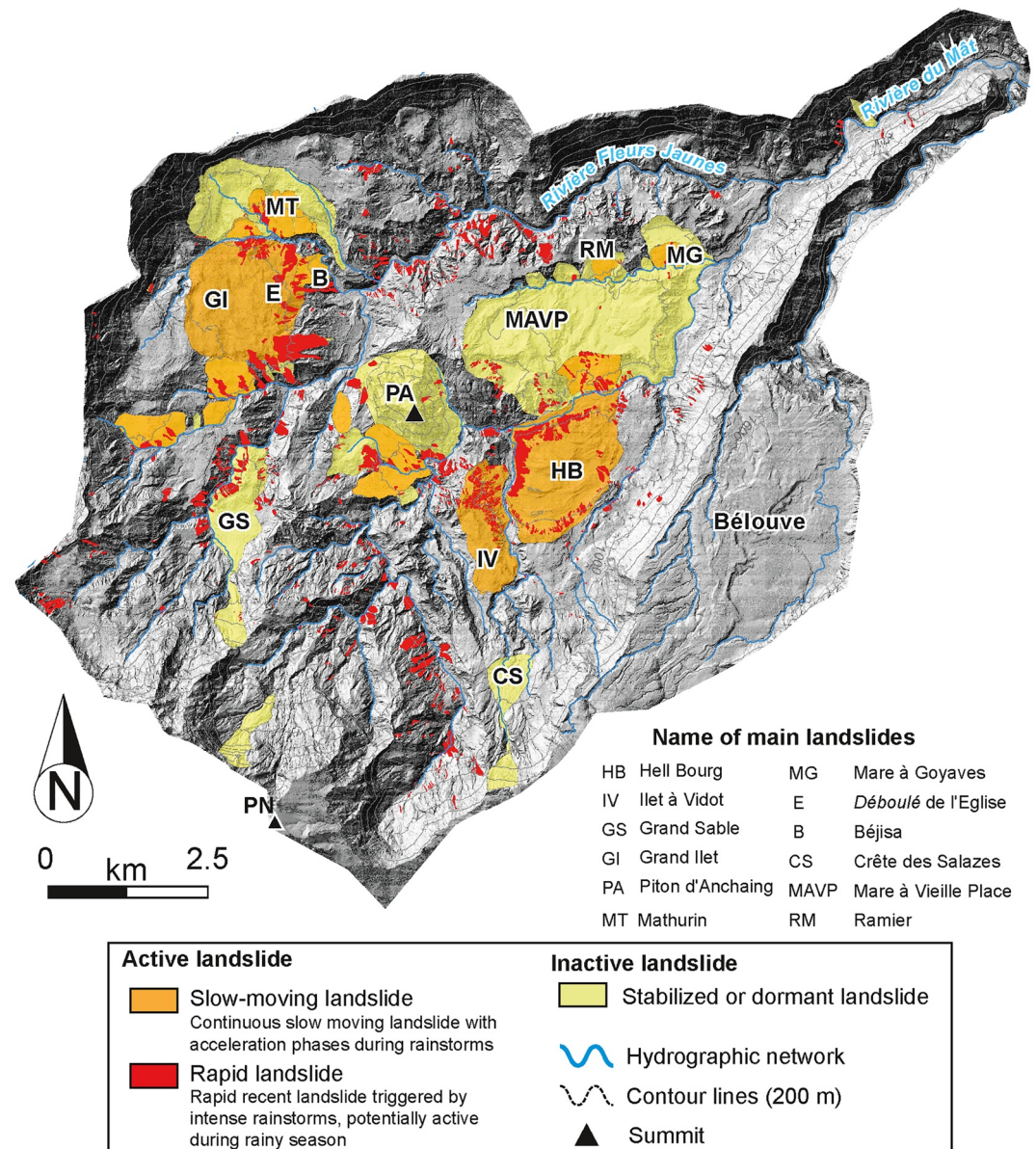
Figure 4. State of recent landslide activity in the Cirque de Salazie. Morphological indices, diachronic analysis of aerial photography, geodetic observations and reports allowed delineation of recently active and inactive landslides. Initials indicate the names of the main landslides and the two main summits of Piton des Neiges (PN) and Piton d'Anchaing (PA). The term recent suggests that morphological evidence of landslide activity is still identifiable in the field.

4.2. Landslide Classification

Eight types of landslides were identified in Salazie (Figure 7). The definition of each type is outlined below and illustrated by a typical example (Figure 8). The distribution of mapped landslide types is given in Figure 5c.

4.2.1. Flows

4.2.1.1. Rock Avalanches (RA)

A rock avalanche can be defined as the sudden failure of a massive volume of rocks ($>10^6$ m^3) that fragments and moves with extreme velocity downslope (Brideau & Roberts, 2015; Hungr et al., 2001, 2014; Figure 7). The failure may initiate along a preferential plane such as a vertical intrusion or a fault. Groundwater may play a role in failure initiation and surficial water in the transportation of the whole mass downslope. Interaction with substrate
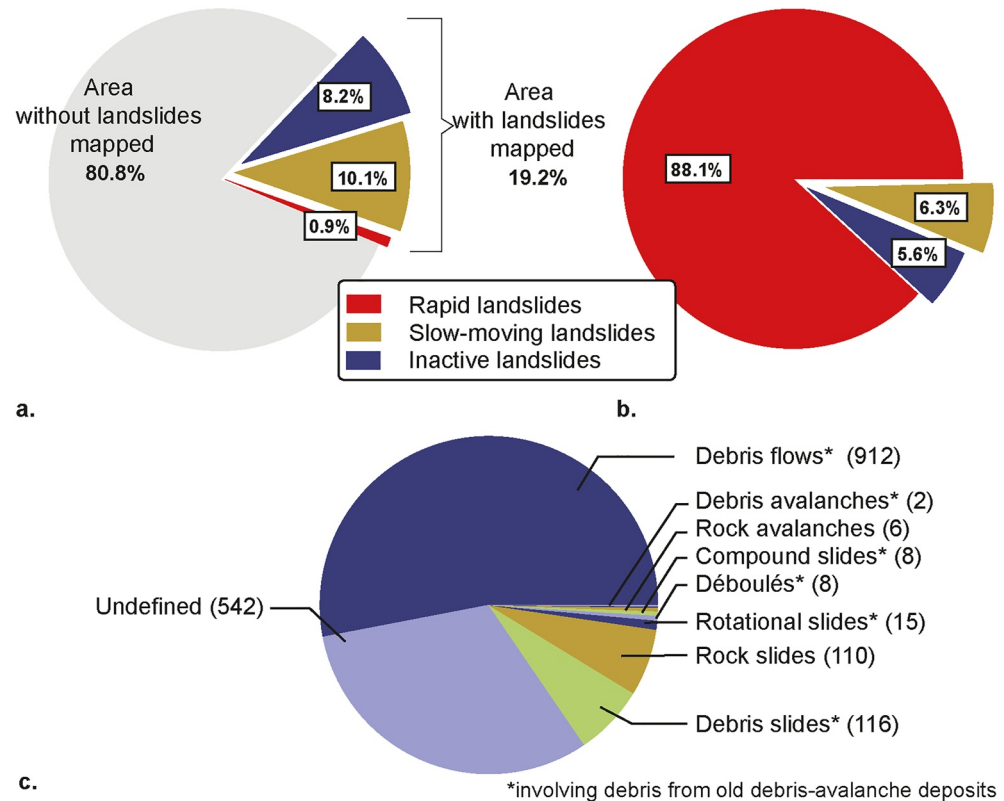
Figure 5. Landslide activity in the Cirque de Salazie. (a) Surface distribution of the state of activity in the *cirque*. The surface covered by landslides is compared to the 3D surface of the cirque (cliffs and center of the depression). According to our landslide inventory, at least 19.2% of the surface of the *cirque* is affected by landslides, with recently active landslides covering at least 11% of its surface. (b) Quantity distribution of the state of activity of mapped landslides in Salazie. A total of 94.4% landslides are recently active (88.1% rapid and 6.3% slow-moving). (c) Quantity distribution of the identified types of landslides, with most of them being debris flows triggered during Cyclone Hyacinthe.

materials also contributes to the mobility of RA (Crosta et al., 2017; Hungr & Evans, 2004). The main deposit of a rock avalanche can be subdivided into two to three facies depending on the volume of material involved: a basal mixed zone, a body composed of fragmented clasts and shear zones, and a surficial zone made of block facies (Dufresne et al., 2016).
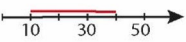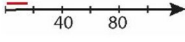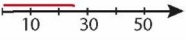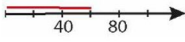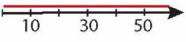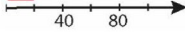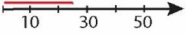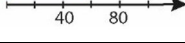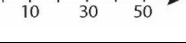
The Grand Sable event is the best known example in Salazie. This rock avalanche occurred in 1875 and buried the small village of Grand Sable, causing the death of 63 people. The deposits covered a distance of more than 2,500 m with thicknesses of up to 40–50 m (Lustremant, 1981). The volume of mobilized material is estimated to be approximately 18×10^6 m^3. A basalt intrusion crops out at the failure surface, dipping north-northeast approximately 70°, and which probably played a significant role in seepage and failure initiation (Humbert et al., 1981; Lustremant, 1981). Since 1875, at least one similar event with lower volume has occurred in the *cirque* (1881—Crête des Salazes—unknown volume, Humbert et al. (1981)).

4.2.1.2. Debris Avalanches (DA)

A debris avalanche is a rapid to extremely rapid flow-like movement (Hungr et al., 2014) of an important volume ($>5 \times 10^5$ m^3) of epiclastic material that suddenly collapses from the steep slopes of *îlet* borders during heavy rainstorms due to excess pore pressure (Figure 7). The material flows downhill at high velocity, eroding and incorporating other slope materials and/or covering gully borders (Pinchinot, 1984). The processes described are much smaller than famous DA occurring on volcano flanks for example. The landslide initiation failure zone is characterized by an unstable steep main scarp, where springs can still gush out several days after the collapse.

Two DA have occurred in Grand Ilet since 1980: one during Cyclone Hyacinthe (1980, volume c. 6×10^5 m^3) and one during Cyclone Bejisa (2014, volume c. 10^6 m^3) (Figure 8b). Both occurred along the steep slopes (>35°) of

Table 2
Characteristics of the Main Slow-Moving Landslides Identified in the Cirque de Salazie

Landslide name	Area (km²)	Mean Topographic Slope (°)	Main direction of displacement	Planimetric velocity (cm.yr⁻¹)	Vertical velocity (cm.yr⁻¹)
Hell Bourg	2.8	15	North	from 20 to 115	from 10 to 40
Ilet à Vidot	0.7	20	Northwest Northwest	from 2 to 15	from 2 to 25
Mare à Goyaves	0.2	25	South	from 2 to 60	from 2 to 60
Mathurin	0.5	35	Southwest	from 2 to 20	from 2 to 25
Grand Ilet	2.5	10	Northeast	from 2 to 55	from 2 to 15

Note. The red cursor illustrates the velocity range of the landslide.

the Grand Ilet landslide boundary and formed distinct scars tens of meters high and gullies that reach and flow into the Rivière des Fleurs Jaunes and Ravine de Roche à Jacquot, respectively. It has been proposed that the removal of materials at the avalanche head resulted in the release of water at the center of the scar, which could have been responsible for the increase in hydrostatic pressure (undrained loading conditions) in the slope material, causing collapse (Humbert et al., 1981).
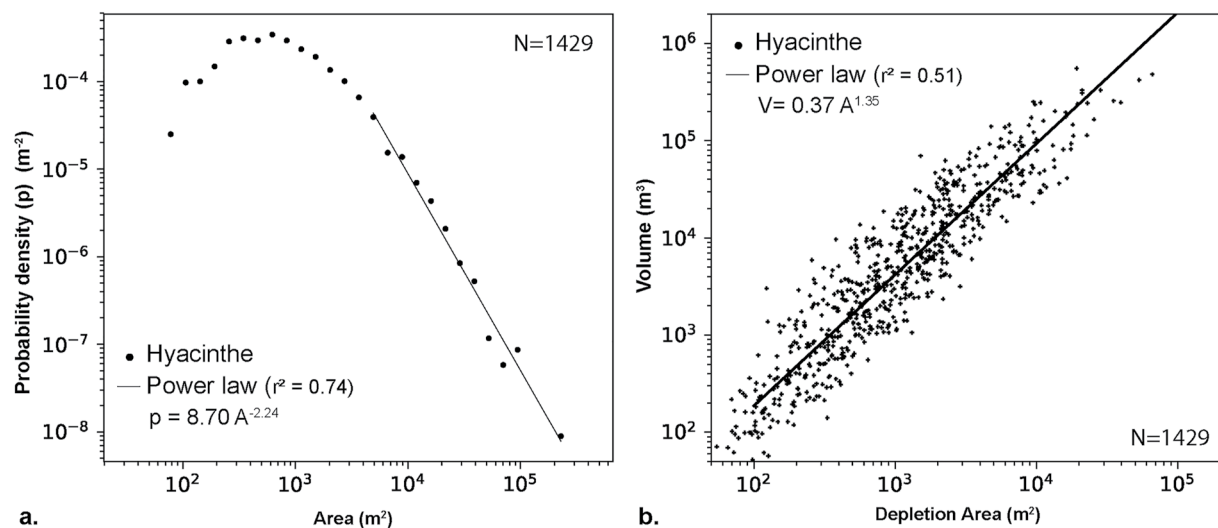
Figure 6. Volume and area of landslides triggered by Cyclone Hyacinthe (1980). (a) Area distribution of landslides. Probability densities (p) are calculated following Malamud et al. (2004) as $P(A) = \frac{1}{N} \frac{\Delta N_l}{\Delta A}$, with ΔN_l the number of landslides of an area comprised between A and $A + \Delta A$. (b) Volume as a function of the landslide depletion area (surface area of the landslide presenting negative heights between 1978 and 1984). The total volume of landslides triggered by Hyacinthe is $15.2 \pm 0.44 \times 10^6$ m³. N: number of landslides considered.
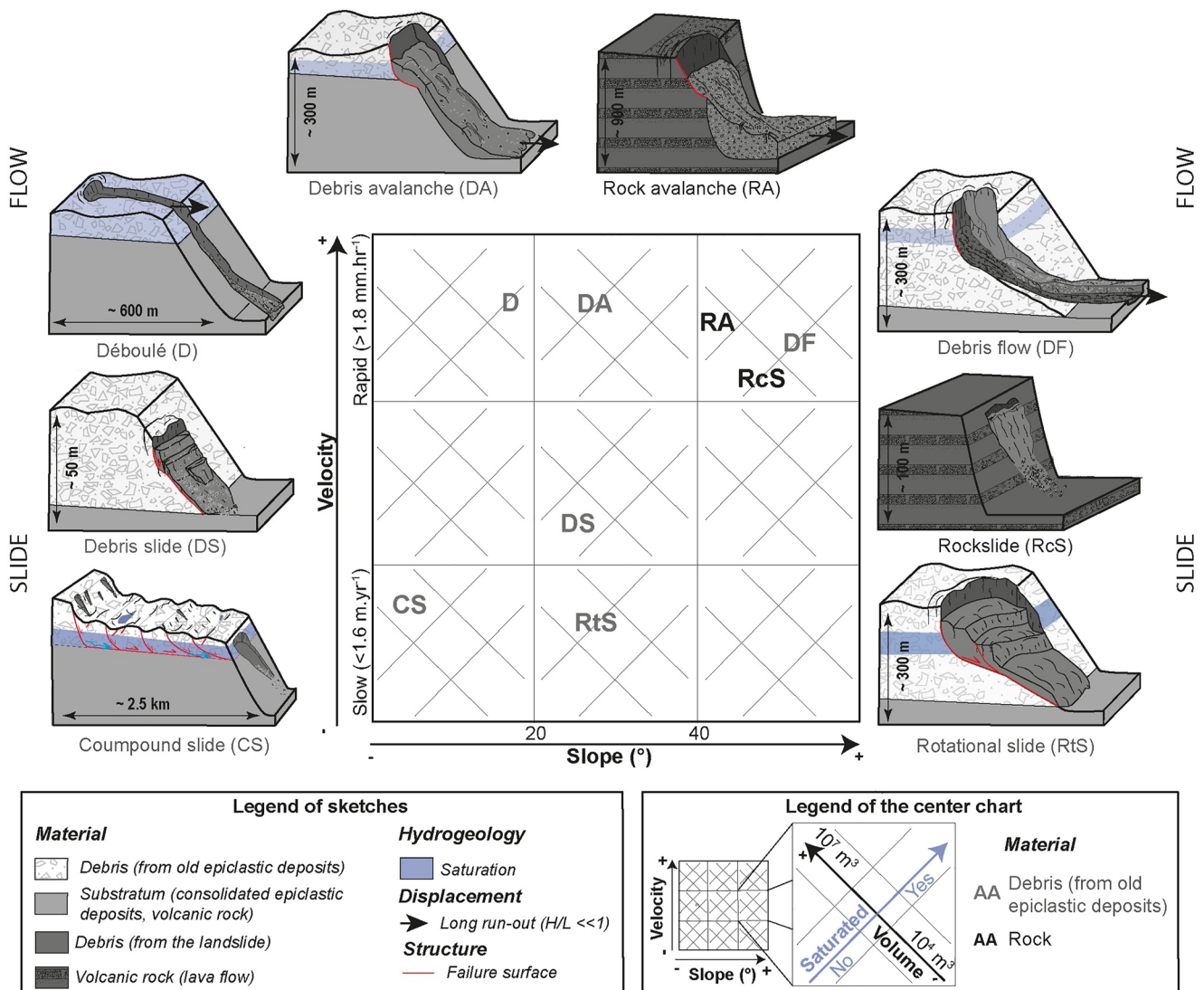
Figure 7. Overview of the eight types of landslides identified in Salazie, which are classified according to their velocity, slope, volume, saturation, involved material, and *H/L* (height of fall (*H*) and the run-out distance (*L*)). Each type is placed in the center chart according to its velocity, slope, volume and saturation. The representative sketches of the landslide types have their own scale. Photos of typical examples illustrate each type in Figure 8.

4.2.1.3. Déboulés (D)

Déboulé is a local term for atypical mass movement of saturated materials observed during very intense rainstorms, which was first described by Humbert et al. (1981). A *déboulé* is a mix of erosion and a flow process that leads to the extremely rapid formation of a gully on a gentle slope <20° (Figure 7; Rault et al., 2022). Indices of internal erosion in depressions support the idea that the formation of a *déboulé* may be initiated by internal erosion of the epiclastic material, leading to ground collapse and bank failure. The saturated failed material flows downslope, intensifying gully erosion.

We identified eight *déboulés* that formed during Hyacinthe (Figure 5c). A representative example of this phenomena is the Ravine de l'Eglise event, which incised a gully approximately 600 m long and 7 m deep in 12 days during Cyclone Hyacinthe on the Grand Ilet Plateau (Figure 8a). Similar smaller features were observed in Grand Ilet's limiting scarps (Figure S4 in Supporting Information S1 and Pinchinot, 1984).
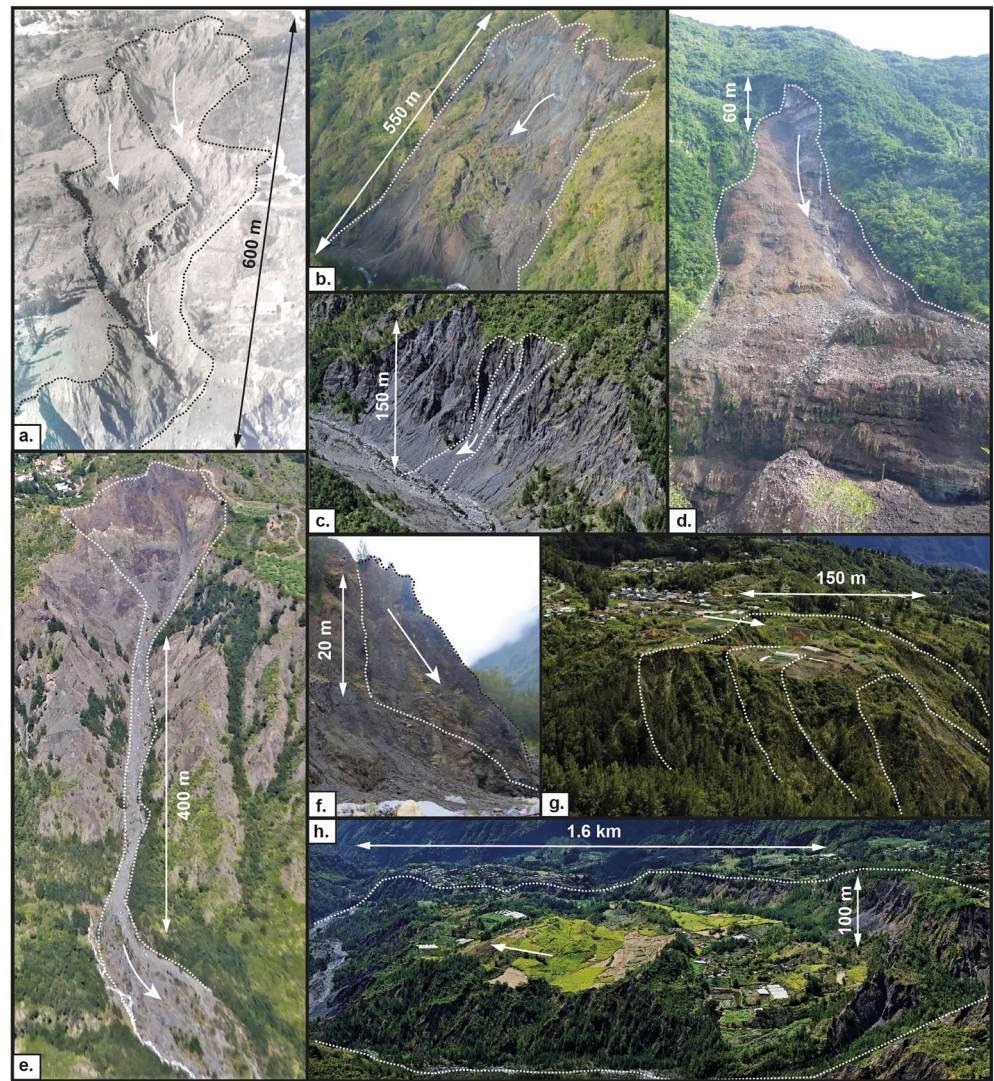
Figure 8. Examples of landslides in Salazie. (a) *déboulé* (Ravine de L'Eglise, 1980), (b) debris avalanche (Béjisa, 2014), (d) rock slide (Ilet Morin, 2010, (c and e) debris flows (c. Rivière du Mât, e. Ilet à Vidot), (f) debris slide (Rivière du Mât), (g) rotational slide (Le Belier), and (h) compound slide (Hell Bourg). The white and black dotted lines delineate landslide boundaries. Arrows show the direction of principal movement.

4.2.1.4. Debris Flows

DF are rapid movements of sorted or unsorted debris characterized by a very long run-out (>100 m) (Hungr et al., 2001; Johnson & Rodine, 1984). The material is saturated or partially saturated (>50%, Iverson et al., 1997). DF can be initiated on abrupt slopes (>40°) of eroded *îlet* borders (small debris flow) or result from the mobilization of debris from previous mass movements (Figure 7). The flowing mass is composed of a mix of boulders and finer particles and moves within a confined path. The resulting lateral deposits along the flow paths are marked by the presence of boulder-rich levées (Blijenberg, 1998; Costa, 1984; Remaître, 2006).

In Salazie, this is the most common landslide type triggered during rainstorms (Figure 5c). They are common along the eastern bank of Ilet à Vidot (Figure 8e), with long run-out deposits and preserved morphological forms (i.e., lateral levées approximately 500 m long and 1–5 m high). Smaller DF are observed on *îlet* borders or along the scars of active landslides (Figure 8c). The volume of materials displaced by DF during TC Hyacinthe ranges from a few 10^2–10^5 m³ (Figure 8c).

4.2.2. Slides

4.2.2.1. Rockslides (RcS)

A rockslide is a rapid movement of a rock mass along a failure surface often located at a structural discontinuity (fault or dyke) or a thin zone of intense strain. The movement begins on a steep to abrupt slope (>40°) and may involve a slide of several m^3 to thousands of m^3 of material (Figure 7).

The basic lava flow sequences crosscut by magmatic intrusions and fault networks forming the scarps of the *cirque* are particularly prone to rockslides. Figure 8d shows the rockslide of Ilet Morin (approximately 1×10^5 m^3) that took place during the 2010 rainy season (Aunay & Rey, 2018).

4.2.2.2. Debris Slides (DS)

A debris slide (DS) corresponds to the sliding of epiclastic materials on a relatively shallow and planar surface along a steep topographic slope (Figure 7). A DS involves a small to moderate amount of material (a few m^3 to hundreds of m^3). Surficial water circulation drives the kinematics of movement.

In Salazie, DSs are identified along landslide crowns, *îlet* borders, and valleys. Failure initiation generally occurs at the interface between different materials on a thin, low-strength layer (e.g., along intrusions or more or less unconsolidated breccia layers). DSs move slowly downslope under normal conditions and may collapse suddenly during intense rainfall, partially due to the increase in water saturation. Figure 8f shows a 20 m-high DS located along the banks of the Rivière du Mât.

4.2.2.3. Rotational Slides (RtS)

RtSs are slow-moving landslides located on moderate to steep slopes (>20°) of epiclastic deposits with arc-shaped sliding surfaces (Figure 7). The ratio of vertical to horizontal displacements is generally close to one. Sliding is favored by an increase in the groundwater level and accelerates beyond a given threshold.

Le Bélier, Mathurin, and Mare à Goyves are examples of rotational landslides in the Cirque de Salazie (Figure 4 and Figure S7 in Supporting Information S1). Figure 8g shows Le Bélier landslide, which consists of successive landslides narrowing toward the Rivière des Fleurs Jaunes. The lower landslide moves in a southwesterly direction between 6 and 10 cm yr^{-1}, while the upper steps are moving more slowly (1.5 cm yr^{-1}).

4.2.2.4. Compound Slides (CS)

A compound landslide is composed of a large host landslide (>10^8 m^3) that encompasses smaller secondary landslides (Figure 7). The host landslide is a slow-moving landslide set on a gentle slope (<20°) of epiclastic materials. Its surface is irregular, with depressions, bulges, scarps and counterscarps and distensile, compressive and strike cracks. The movement of the host landslide can generate failures that favor secondary landslides located mostly along the steepest slopes of the host landslide (scarps and toe). Diverse types of secondary landslides may be observed on the same host landslide.

Multiple levels of groundwater flow are commonly formed within compound landslides due to the presence of multiple low permeability surfaces (faults, cracks, material heterogeneities, and shear planes). An increase in the water table tends to accelerate host landslides and may contribute to secondary landslide failure.

In Salazie, three large compound landslides (>0.2 km^3) can be observed: Grand Ilet, Hell Bourg (Figure 8h) and Ilet à Vidot, each with its own structure and dynamics (Belle, 2014; Haurie, 1987; Humbert et al., 1981; Rault et al., 2021). The next section provides a detailed description of them.

4.3. Morphodynamics and Structure of Three Large Compound Landslides

Grand Ilet, Hell Bourg and Ilet à Vidot are three major inhabited compound landslides of Salazie. These landslides move continuously and accelerate following heavy rainfall (Figure 9). They occupy approximately 10% of the *cirque*'s surface area (Figure 5a) and therefore represent a significant hazard. Understanding their structure, their dynamics and their involvement in the formation of secondary landslides is essential for hazard and risk mitigation.
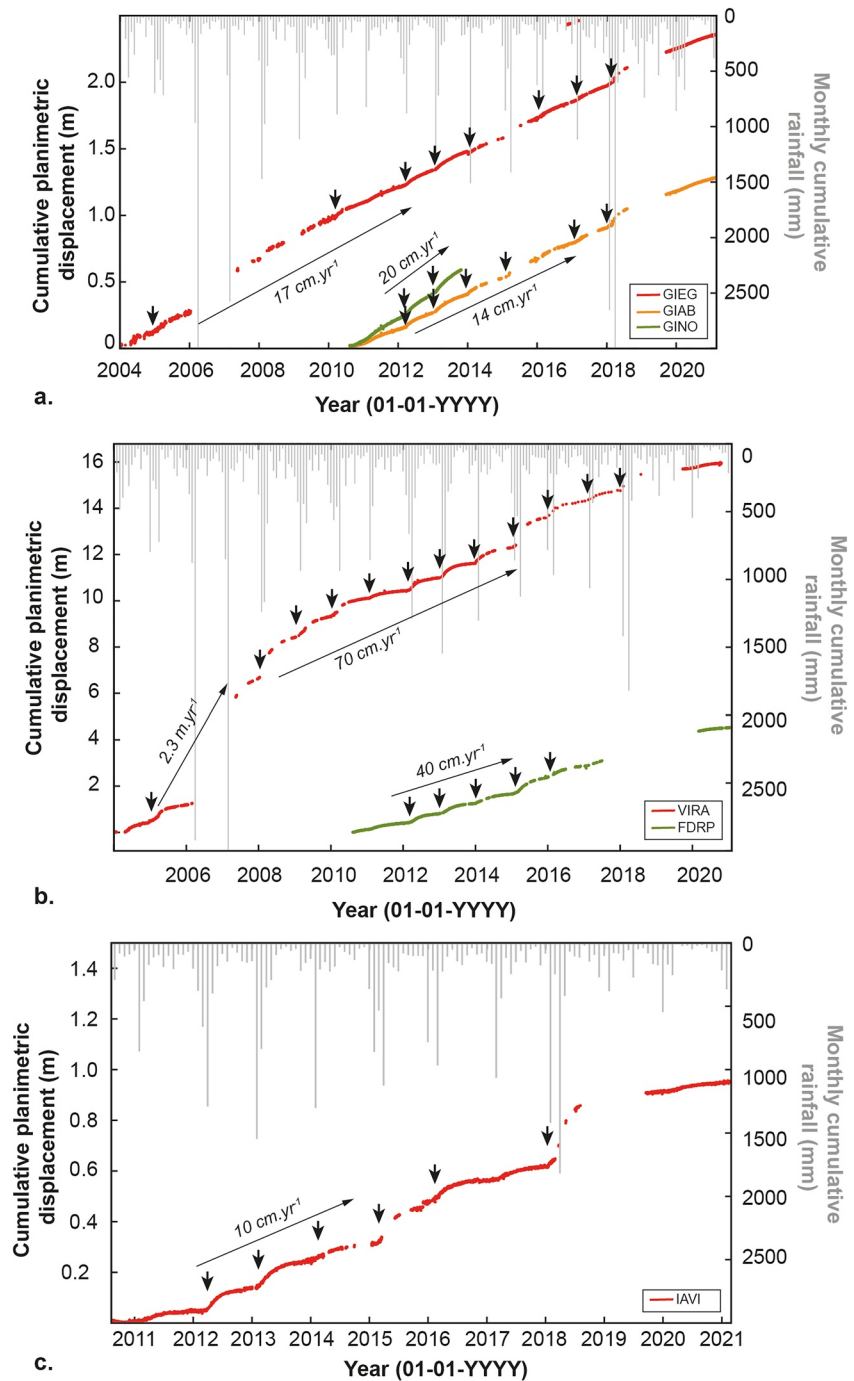
Figure 9. Cumulative planimetric displacements of the three compound landslides studied, measured with global navigation satellite system (GNSS) stations from 2004 to 2021, and monthly rainfall at (a) Grand Ilet landslide, (b) Hell Bourg landslide, and (c) Ilet à Vidot landslide. Acceleration (thick black arrows) of the movement occurs during the wet season after intense rainfall. The locations of the GNSS stations on Grand Ilet (GIAB, GIEG, and GINO), Hell Bourg (VIRA and FDRP) and Ilet à Vidot (IAVI) are shown in Figures 10, 12 and 14, respectively.

Based on morphological indices, AEMs, and borehole data, and previous studies listed in Table S1 in Supporting Information S1 we propose a detailed description of their surface and internal structure.

4.3.1. Grand Ilet Landslide

4.3.1.1. Grand Ilet: Surface Morphology and Landslide Activity

The Grand Ilet landslide covers an area of ~2.5 km² and is up to 2 km long and 1.8 km wide (Figure 10; Belle, 2014; Pinchinot, 1984), The average slope of the moving mass is around 10°. The surface is made up of successive scarps that are tens of meters to a few meters high and oriented NW-SE. The Grand Ilet landslide moves toward the northeast with horizontal velocities ranging from 0.02 m yr⁻¹ at its head to 0.55 m yr⁻¹ close to its toe (Figures 9a and 10). The vertical velocities are too small to be measured at its head and are about 0.15 m yr⁻¹ at its toe. Velocities exhibit seasonal variations, with acceleration after intense rainfall (Figure 9a).

Many cracks and other damage to infrastructure resulting from this displacement are observed in Grand Ilet (Figure S8 in Supporting Information S1). Local velocity changes induce the formation of compression and extension cracks, mainly oriented NW-SE. Depressions and counterslopes oriented NW-SE are probably the result of the landslide's overall extension. Two main families of conjugate shear cracks are identified, oriented N70 and N120. These shear cracks separate landslide compartments with different velocities. Most of the current morphological features have a direction consistent with the orientation of the local extensional paleostress regime, determined from intrusions and old deformation structures (Chaput et al., 2014, 2017).

The toe and steep scarps of the Grand Ilet landslide are affected by secondary landslides (e.g., DA, *déboulés*, DF) that may contribute to the host landslide's mobility due to erosion of lateral margins (Figure 10).

Permanent streams are rare in the Grand Ilet plateau. Rainfall infiltrates mainly along the western scarp of the *cirque* (Belle, 2014). Water then flows into the epiclastic units, including those of the landslide body, and recharges the Grand Ilet aquifer. Groundwater emerges as permanent springs along the northern and, to a lesser extent, the eastern limits of the landslide on steep slopes and gullies. Precipitation at Grand Ilet can also accumulate in closed depressions (ponds, grabens, and undefined closed depressions) and then slowly infiltrate the landslide body (Belle et al., 2014; Humbert et al., 1981; Pinchinot, 1984).

4.3.1.2. Grand Ilet: Internal Structure

The analysis of all available data led to a conceptual model of the internal structure of the Grand Ilet landslide (Figure 11).

The sliding mass is made up of a heterogeneous poorly consolidated epiclastic material called Grand Ilet Breccia. This unit is set on an older indurated epiclastic deposit. Once weathered, the indurated epiclastic deposit turns into a low-strength blue-gray clay that often crops out along the sliding surface. The three piezometers located in Grand Ilet are sheared. The depth of shear (PZA3 ~84 m, PZE2 ~66 m, and PZB3 ~86 m) can be interpreted as the base of the landslide. At the front of the landslide, in Ravine Roche à Jacquot, the limit between the sliding and the stable mass can be identified by a lithological change from indurated to non-cohesive epiclastic deposits of the Grand Ilet Breccia at approximately 900 m a.s.l. (Belle et al., 2014). Springs appear all along this limit, especially after heavy rainfall (Figure S9 in Supporting Information S1). According to these observations, the shear surface of the landslide ranges between 50 and 150 m in depth. This limit corresponds to a resistivity of c. 80 Ω m in the 3D resistivity model (Figure S10 in Supporting Information S1). The landslide material is more porous than the substratum due to the displacement of the landslide (Belle, 2014; Pinchinot, 1984). Thus, for the same lithology (Grand Ilet Breccia), the landslide material appears more resistive than the stable material of its substratum.

Considering the surface area and depth of the delineated landslide base, the sliding mass (>80 Ωm) has a calculated volume of approximately 2.15×10^8 m³.

It is composed of two resistive units of the Grand Ilet Breccia: GIB_1 and GIB_2 (Figure 11b). The highest resistive unit GIB_1 (>200 Ωm) is approximately 50–100 m thick and crops out at the surface along the main escarpments. GIB_2 (80 Ωm < r < 200 Ωm) is separated into two layers. The less resistive unit (80 Ωm < r < 120 Ωm), between 1,100 and 850 m a.s.l., may correspond to the aquifer in agreement with the piezometric survey. Above, the less resistive layer (120 Ωm < r < 200 Ωm) would therefore correspond to a less saturated zone. GIB_2 is predominant and crops out downstream of the landslide where the matrix facies of the Grand Ilet Breccia is mostly observed.
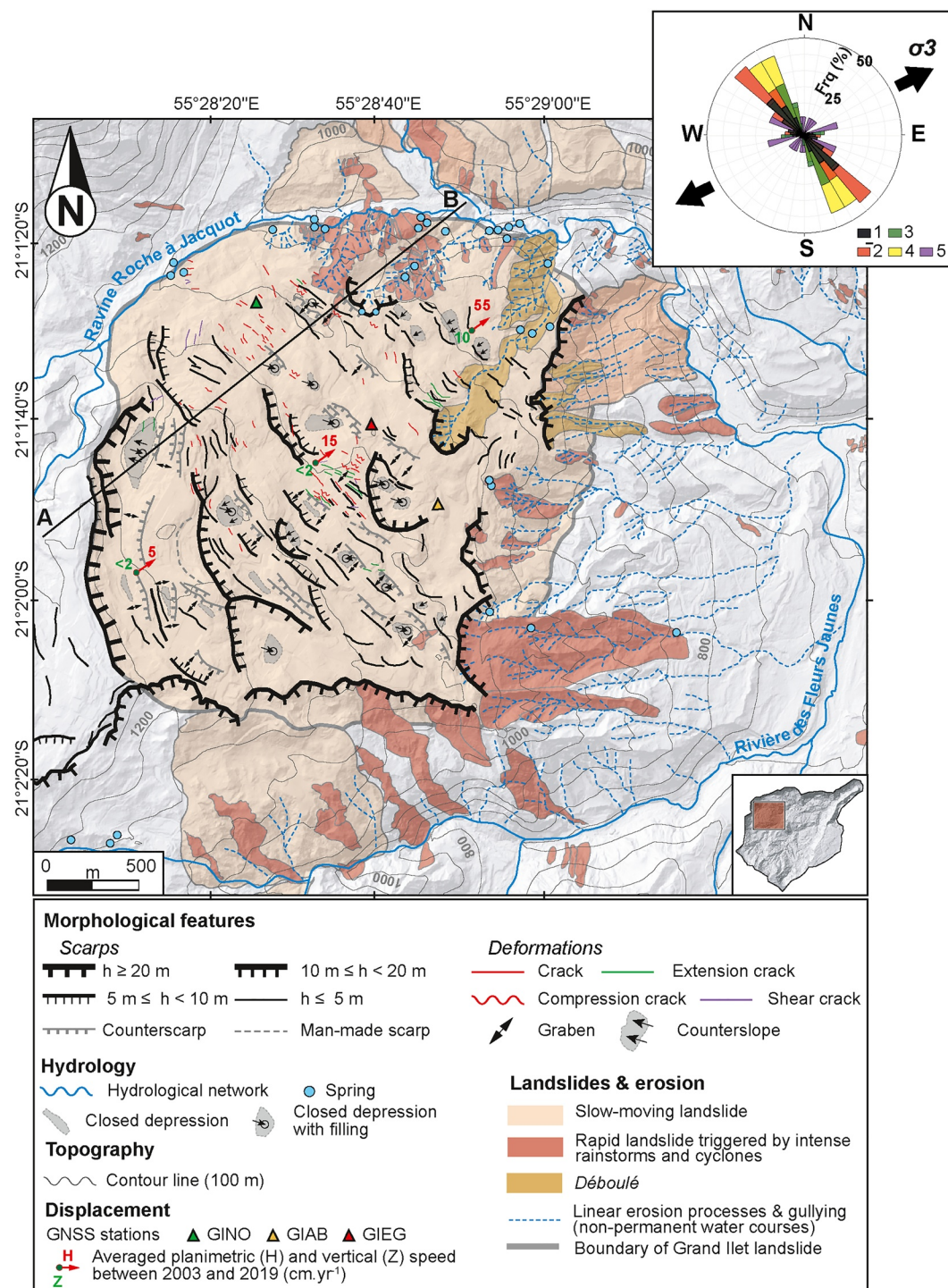
Figure 10. Morphology of the Grand Ilet landslide. The black line A–B marks the ends of the cross-section presented in Figure 11. The rose diagram shows the direction of the scarps (1) and the deformation structures (2: undefined cracks, 3: extension cracks, 4: compression cracks, and 5: shear cracks). The thick black arrows next to this diagram indicate the local direction of paleoextension $\sigma3$ determined by Chaput et al. (2014).
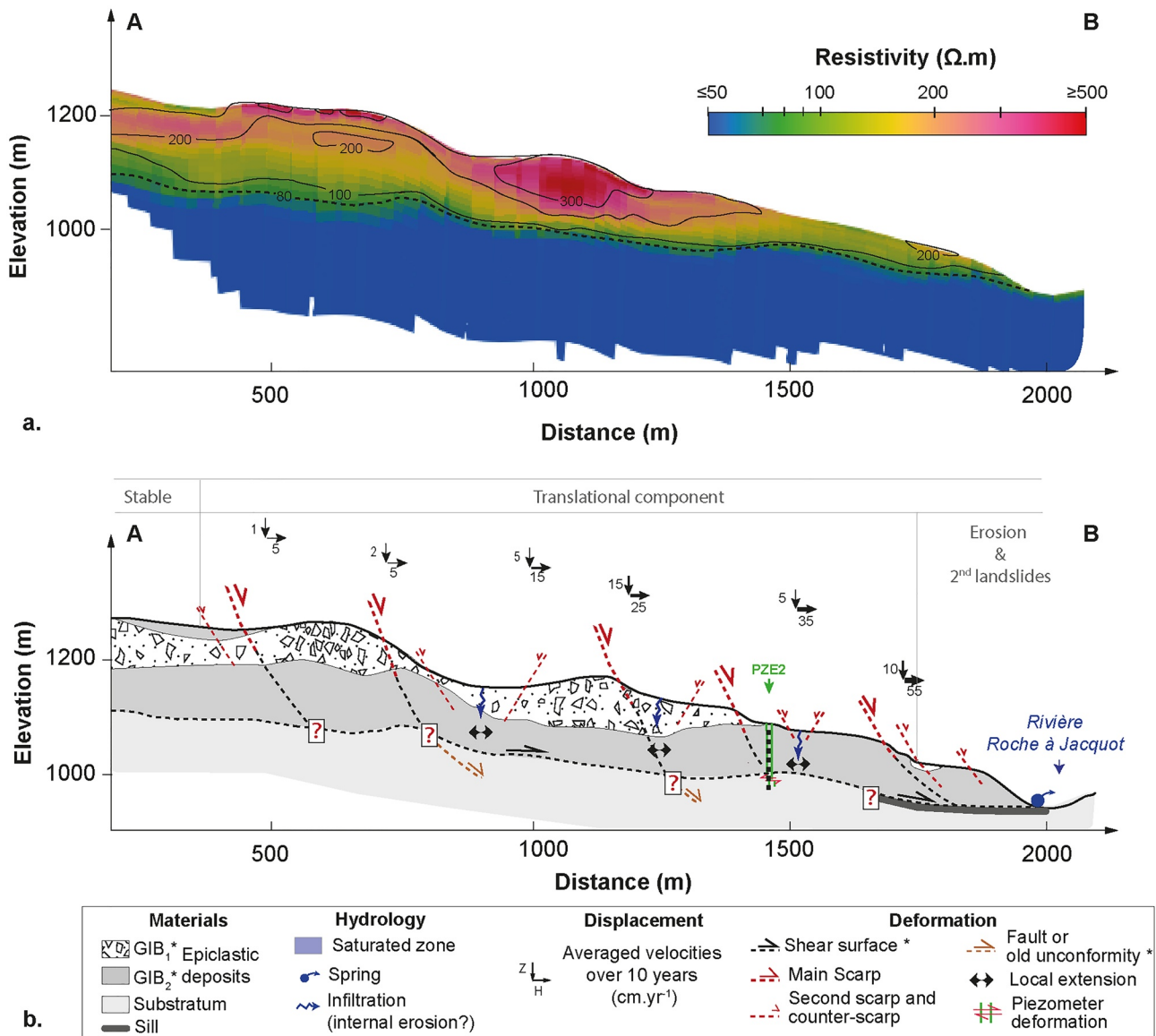
Figure 11. Interpretation of the internal structure of the Grand Ilet landslide along profile A–B located in Figure 10. (a) Resistivity model of Grand Ilet along A–B obtained from AEM data. The isoresistivity contours are drawn with black lines. The 80 Ωm limit is interpreted as the landslide slip surface. (b) Conceptual morphodynamic cross-section of the landslide obtained through a compilation of the available data (see Section 3). Symbol * means that the feature is deduced mainly from geophysical data. Question marks indicate where uncertainties remain about the depth and location of internal structure features. GIB₁ and GIB₂: facies of the Grand Ilet Breccia.

More investigations should be undertaken to associate GIB_2 and GIB_1 to facies of the Grand Ilet debris-avalanche deposits.

Two main slope breaks can be observed on the resistivity model along the sliding surface. Their nature and connection with the main scarps at the surface remain unclear but may be interpreted as major unconformities in the landslide body.

The lateral resistivity gradient occurring in small depressions close to the scarps, together with counterscarps on the surface, may attest to local internal extension of the landslide body resulting from acceleration toward the northeast. This acceleration is possibly linked to secondary landslides and rapid erosion processes occurring at the landslide's toe (Figures 4, 10 and 11). During intense rainfall, these depressions can fill with water. Their

drainage into the landslide body may induce internal erosion and influence the formation of secondary landslides such as *déboulés*.

4.3.2. Hell Bourg Landslide

4.3.2.1. Hell Bourg: Surface Morphology and Landslide Activity

Hell Bourg is a compound landslide covering a surface of approximately 2.8 km^2 (maximum 2 km long and 1.5 km wide). The average slope of the main landslide body is approximately 15° (Arnaud, 2005; Rault et al., 2021).

Geodetic data show that the Hell Bourg landslide experiences overall northward stretching. It moves slowly toward the Rivière du Mât with planimetric velocities ranging from 20 cm yr^{-1} at its crown to 1.15 m yr^{-1} close to its toe (Figures 9b and 12). The vertical velocities average 10 cm yr^{-1} on the main landslide body and reach up to 40 cm yr^{-1} at its crown. They are highest at its head where the vertical component is dominant. The velocity experiences seasonal variations, with acceleration after intense rainfall (Figure 9b; Belle, 2014; Belle et al., 2018).

The head of the landslide is characterized by a main scarp of approximately 120 m in height, covered by debris from small landslides. The landslide crown presents large cracks oriented between N50 and N80 (Figure 12 and Figure S11 in Supporting Information S1). These cracks are caused by vertical movements (up to 40 cm yr^{-1}) of large blocks (up to 100 m behind the crown) that may result in multiple retrogressive small to large retreats of the crown (Figure S11 in Supporting Information S1), as occurred during Cyclone Hyacinthe (Humbert et al., 1981). The crown of the landslide southwest of the pond of Mare à Poule d'Eau is affected by a retrogressive slow-moving rotational landslide attested by scarps (10–20 m high) and extension cracks.

The landslide toe crops out in the valley of the Rivière du Mât. It is characterized by an active bulge marked by large open cracks (>20 cm) oriented N50-N80 (Figure S12 in Supporting Information S1). The river incises the landslide without reaching its base. The incision results in the formation of steep badland slopes up to 100 m high affected by numerous secondary landslides and rapid erosion processes.

The landslide body is composed of two major compartments, a western and an eastern part, separated by a sinistral shear zone that accommodates faster displacements of the eastern compartment. The western compartment comprises three ridges that are 30–50 m high, 150–250 m wide, and approximately 500 m long. Geodetic measurements, DEM analysis and field observations suggest that these ridges experience local compression (N90-N120 compression cracks) (Figure 12 and Figures S13–S15 in Supporting Information S1) and local sinistral shear (N30-N60 shear cracks) (Figure 12).

The eastern compartment can be separated into three zones from south to north. The southern zone is characterized by aligned ridges similar to the western compartment ridges; the center of the eastern compartment is marked by a large depression containing the pond of Mare à Poule d'Eau; and the northern part is the most active area of the Hell Bourg landslide, with displacements of up to 1.14 m yr^{-1} inducing considerable damage to infrastructure. A dense network of compression cracks oriented N70, intersected by N30-N50 shear cracks, is observed at the limit between the central depression and the most active part of the landslide.

A few springs with very small flows emerge along the northern flank of the landslide in the western part, while larger flows emerge on the eastern part of the landslide feeding the pond of Mare à Poule d'Eau. Since Cyclone Hyacinthe (1980), this pond has been drained by a permanent stream that runs from the pond to the river along the eastern main scarp of the landslide. There is no other permanent stream on Hell Bourg, suggesting that water flows mainly underground. Water from the pond of Mare à Poule d'Eau may seep into the landslide, thus contributing to groundwater recharge and favoring the displacement of the northeastern part of the landslide.

As a whole, the morphological features of the landslide follows the main paleoextension orientations determined by Chaput et al. (2014) on faults.

4.3.2.2. Hell Bourg: Internal Structure

From the analysis of morphological structures and AEM data, we propose a conceptual model of the internal structure of the Hell Bourg landslide (Figure 13).

The Hell Bourg landslide is composed of epiclastic material of the Mare à Poule d'Eau Breccia. In some places, the epiclastic deposits contain megaclasts made of intensely fractured lava flows with jigsaw cracks whose original stratigraphic structure (alternation of reddish brecciated layers and of grayish massive lava units) is still
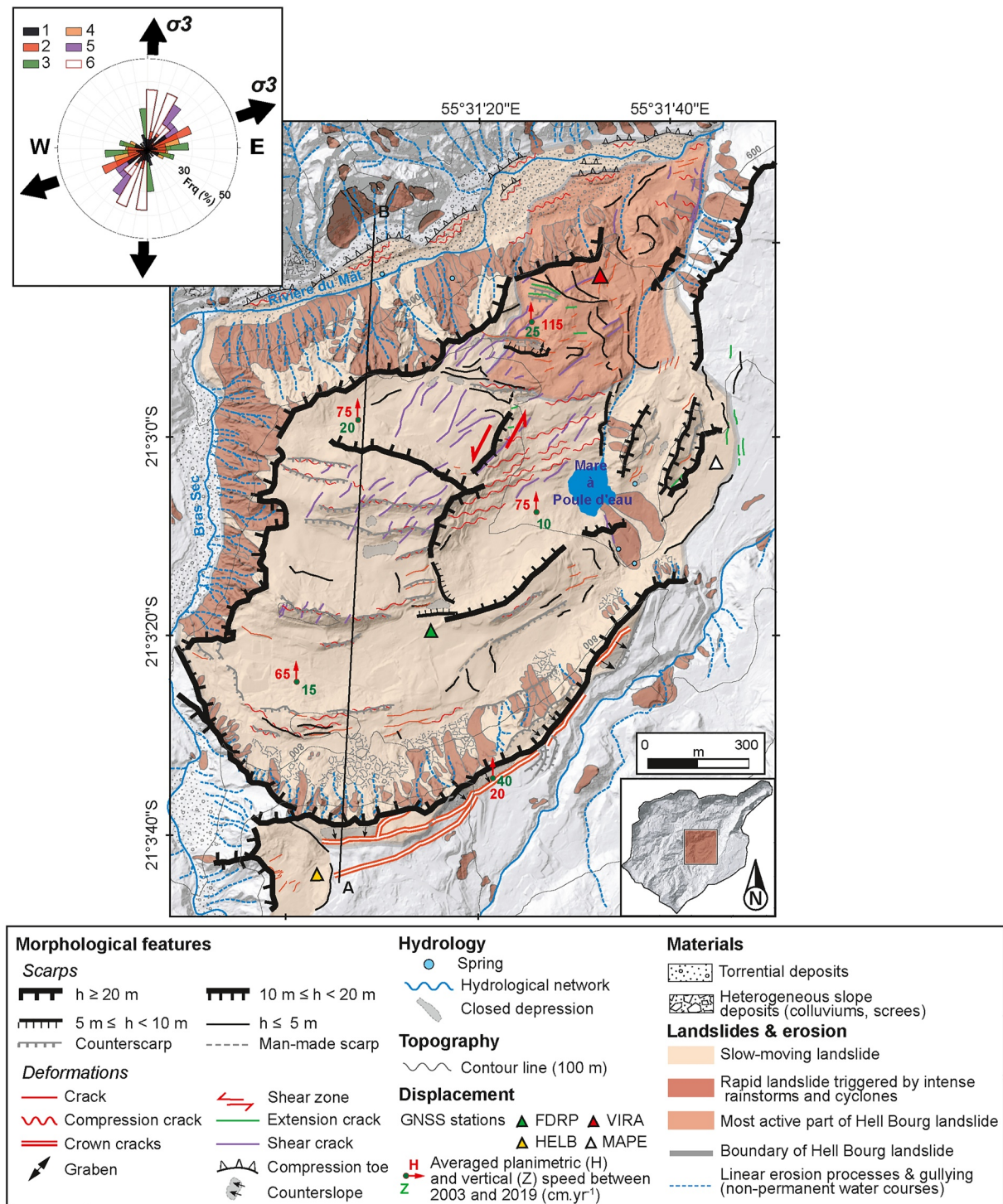
Figure 12. Morphologic map of the Hell Bourg landslide. The black line A-B indicates the location of the cross-section presented in Figure 13. The rose diagram shows the direction of the scarps (1) and deformations observed in the field (2: cracks, 3: extension cracks, 4: compression cracks, 5: shear cracks, and 6: crown cracks). The black arrows next to this diagram are the paleoextensions σ3 determined by Chaput et al. (2014).

discernible (Figure S2 in Supporting Information S1). The moving mass overlies an older breccia unit containing ignimbrite fragments. The contact between these two formations is observed in the Rivière du Mât and matches with the continuous limit of approximately 50 Ωm resistivity, drawn on the resistivity profile presented in Figure 13a. Therefore, we interpret this limit as the main base of the landslide. This surface is at a depth of
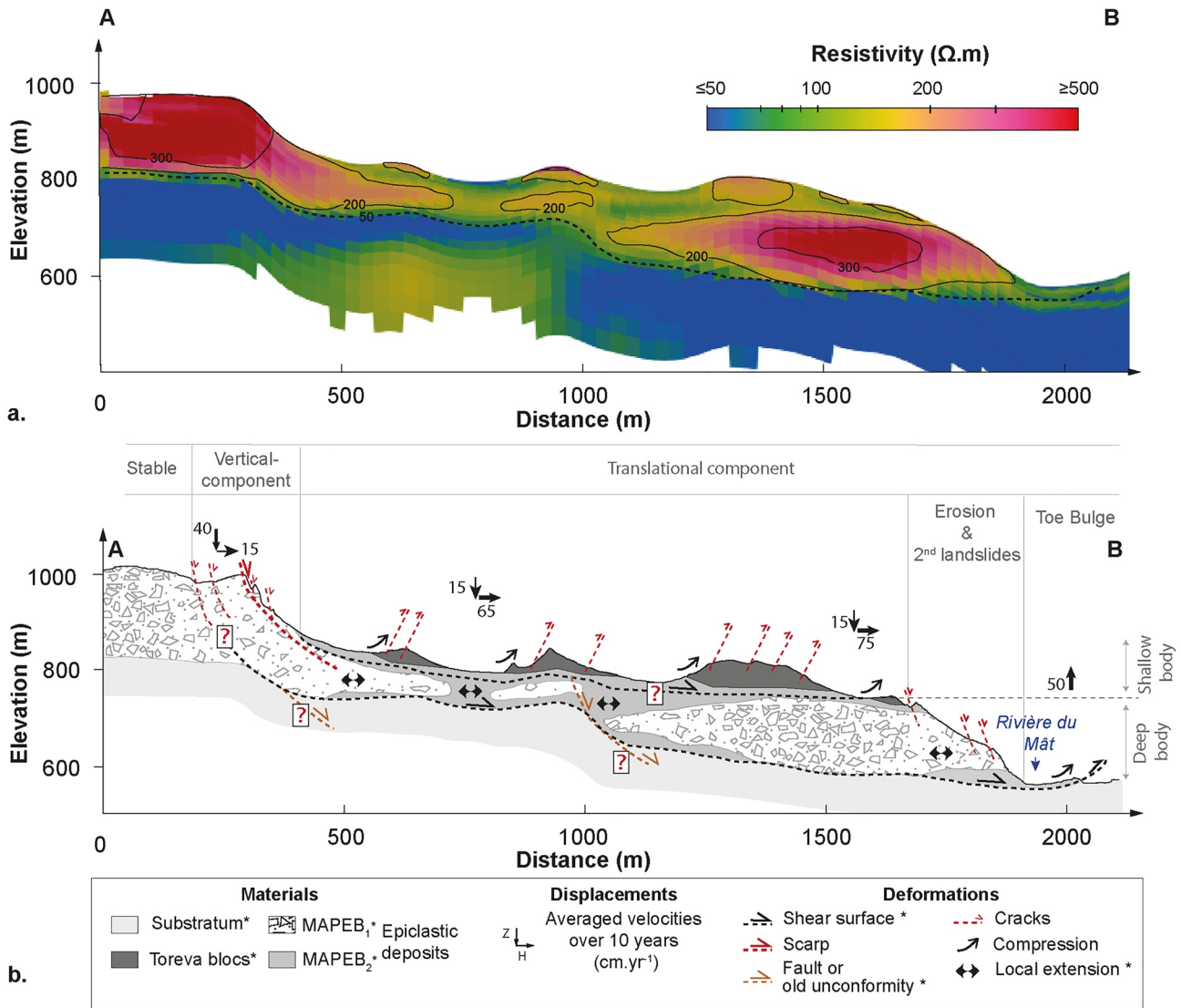
Figure 13. Interpretation of the internal structure of the Hell Bourg landslide along profile A–B in Figure 8. (a) Resistivity model of Hell Bourg along A–B obtained from AEM data. The dashed black line corresponds to the interpreted landslide slip surface, and the solid black line corresponds to the isoresistivity contours. (b) Conceptual morphodynamic cross-section of the landslide obtained using a compilation of the different data available (see Section 3). Symbol * means that the feature is deduced mainly from geophysical data. Question marks are located where uncertainties remain regarding the depth and location of internal structure features. $MAPEB_1$ and $MAPEB_2$: facies of the Mare à Poule d'Eau Breccia.

c. 200 m in the northern part and c.100 m in the southern part of the landslide (Figure 13a and Figure S15 in Supporting Information S1). The landslide base, along profile A–B, is marked by two major steps, above which the resistivity in the landslide body is reduced and the topographic surface of the landslide is marked by small depressions. These steps seem to be aligned with the landslide scarps observed at the surface, suggesting that the location of the landslide base may be influenced by the paleotopography.

The volume of the Hell Bourg landslide, estimated from surface and internal analyses, is about 2.25×10^8 m^3.

The landslide body is composed of two main groups of materials of the Mare à Poule d'Eau Breccia: $MAPEB_1$ and $MAPEB_2$. $MAPEB_1$ has a resistivity of above 150 Ωm. $MAPEB_1$ crops out along the main scarp and the northern steep slopes of the landslide where lava flow megacasts are observed. $MAPEB_2$ has a lower resistivity than $MAPEB_1$ (50 Ωm < r < 150 Ωm). It fills the spaces between the blocks of $MAPEB_1$, particularly where topographic depressions are mapped. Thus, $MAPEB_1$ might correspond to a megacast-rich facies of the MAPE debris-avalanche deposits, in contrast to $MAPEB_2$, which might represent a matrix or mixed facies.

On the resistivity profile, the three ridges observed at the surface appear to be isolated structures. Their resistivities range from 150 to 500 Ωm, the same resistivity range as for the main scarp of the landslide (MAPEB$_1$). Their calculated volumes range from 3×10^6 to 10×10^6 m^3. Because of their resistivity, together with the morphology and activity of the landslide's main scarp, we suggest that these ridges result from multiple massive retrogressive collapses of the main scarp and may therefore be akin to toreva blocks (Reiche, 1937).

To the north of the profile, two superimposed resistive layers ($r > 100$ Ωm) of a thickness of c. 70 m are observed. The interface between these two layers has low resistivity. Small springs are located at the same elevation level as these low resistive layers along the northern talus slope of the landslide. These springs are evidence of groundwater flows, which may explain the low resistivity in this area due to higher water content and possible material alteration.

Lateral decreases in resistivity immediately below the topographic depressions, observed at the surface between the ridges, could be interpreted as a local zone undergoing rapid extension. Topographic depressions, as preferential zones of water infiltration, may experience local pore pressure increases that may locally affect landslide kinematics by favoring displacement of the material. Complementary information on this specific landslide can be found in Rault et al. (2021).

4.3.3. Ilet à Vidot Landslides

4.3.3.1. Ilet à Vidot: Surface Morphology and Landslide Activity

The active plateau of Ilet à Vidot is located northwest of Hell Bourg and covers an area of 2.3 km^2. It is approximately 2.4 km long and 0.9 km wide.

The plateau of Ilet à Vidot is being dismantled on both sides by landslides moving either eastward or westward. The eastern part of the plateau is moving toward Ravine du Bras Sec at a velocity ranging from about 2 to 10 cm yr^{-1}, with vertical movement (subsidence) of 2–25 cm yr^{-1}. These displacements accelerate in response to rainfall (Figure 9c). The northwestern part of the plateau is moving toward the Rivière du Mât at c. 15 cm yr^{-1}, with a vertical displacement of 7 cm yr^{-1} (Figure 14).

The topography of Ilet à Vidot is irregularly marked by numerous high scarps ($h > 10$ m), especially in the northern part. Most of the scarps are oriented northwest–southeast, that is, mostly perpendicular to the local paleoextension N10 determined by Chaput et al. (2014).

Several directions of cracks were observed and mapped, which are mostly oriented northwest-southeast (N130) in the center and lateral part of the plateau, and east-west (N90) in its southern zone. In the southern part of the plateau, the extension cracks are also consistent with local paleoextension N10.

The borders of the *îlet* are affected by numerous secondary landslides, such as DF and localized DSs. The eastern and western borders of the *îlet* are incised by recurrent DF, and their main scarps are on the verge of joining up, thus separating the northern part of the *îlet* from the southern part. These secondary processes favor the overall instability of the plateau and more considerable movements.

4.3.3.2. Ilet à Vidot: Internal Structure

Ilet à Vidot plateau is made of epiclastic material of the Ilet à Vidot Breccia and undifferentiated epiclastic units. On outcrops located along eroded slopes, mixed and megaclast-rich facies of ancient large DA are observed. Megaclast-rich facies, for example, contains megaclasts of intensely crushed lava flows with preserved original stratigraphy/structure.

Figure 15 shows the resistivity profile across the A–B west-east section of Ilet à Vidot plateau indicated in Figure 14. This profile cuts the western and eastern slow-moving landslides that are represented in blue and tan, respectively, in Figure 14.

The apparent resistivity at 100 Ωm seems to correspond to the limit between the landslide ($r > 100$ Ωm) and stable materials ($r < 100$ Ωm). The base of the active body is close to the surface in the riverbeds and approximately 150 m thick in the middle of the plateau.
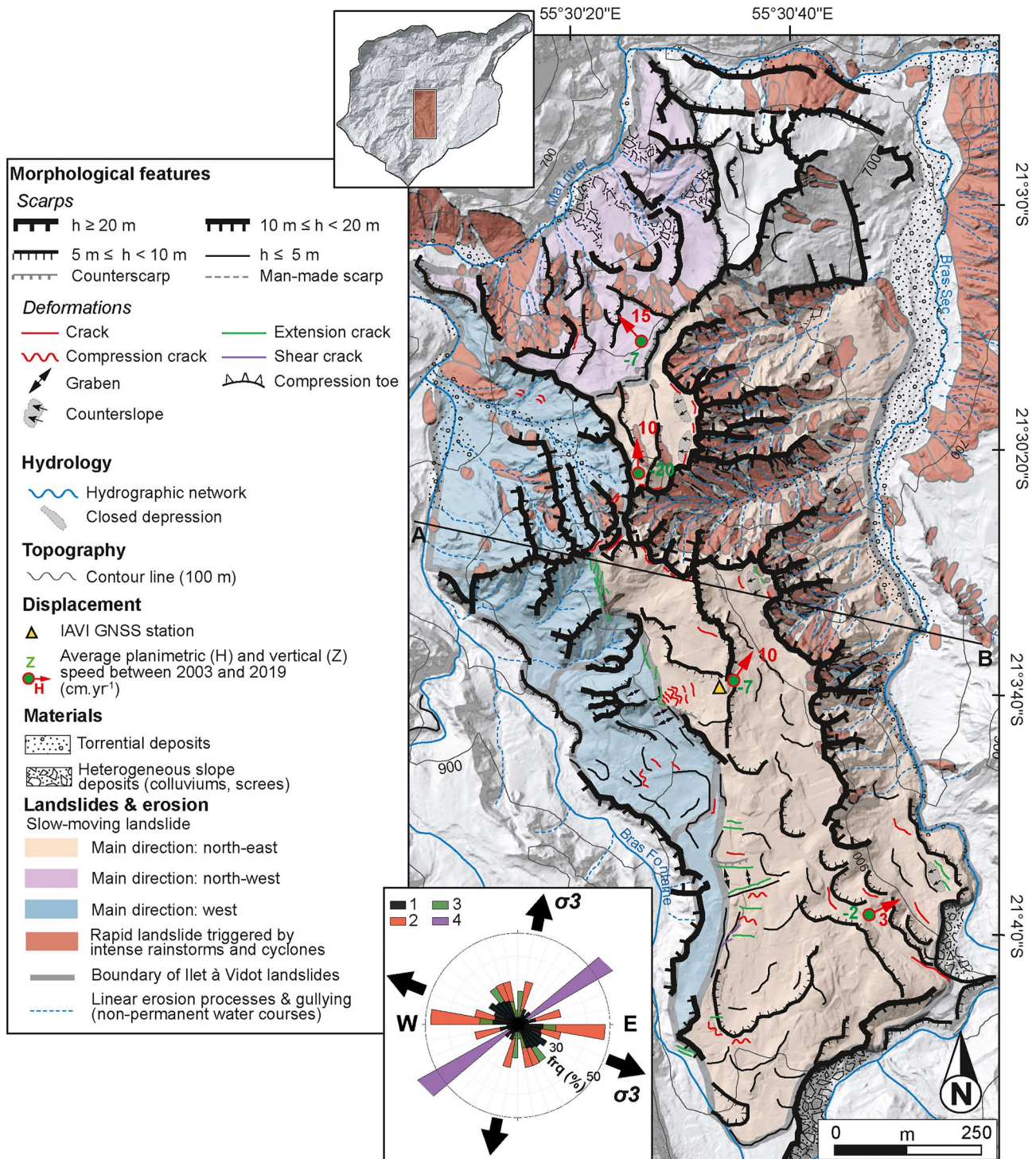
Figure 14. Morphologic map of the Ilet à Vidot landslide. The black line A–B indicates the location of the cross-section presented in Figure 15. The rose diagram shows the directions of the scarps (1) and the deformation (2: unspecified and compression cracks, 3: extension cracks, and 4: shear cracks). Only two shear cracks are identified and mapped, and therefore their distribution is not representative. The black arrows next to this diagram indicate the local direction of paleoextensions $\sigma3$ determined by Chaput et al. (2014).

The active body is composed of two resistivity groups: IVB_1 ($r > 200$ Ωm) and IVB_2 (100–200 Ωm). As for the Hell Bourg and Grand Ilet landslides, IVB_1 might correspond to a megablock-rich facies, while IVB_2 to a mixed facies of debris avalanche.
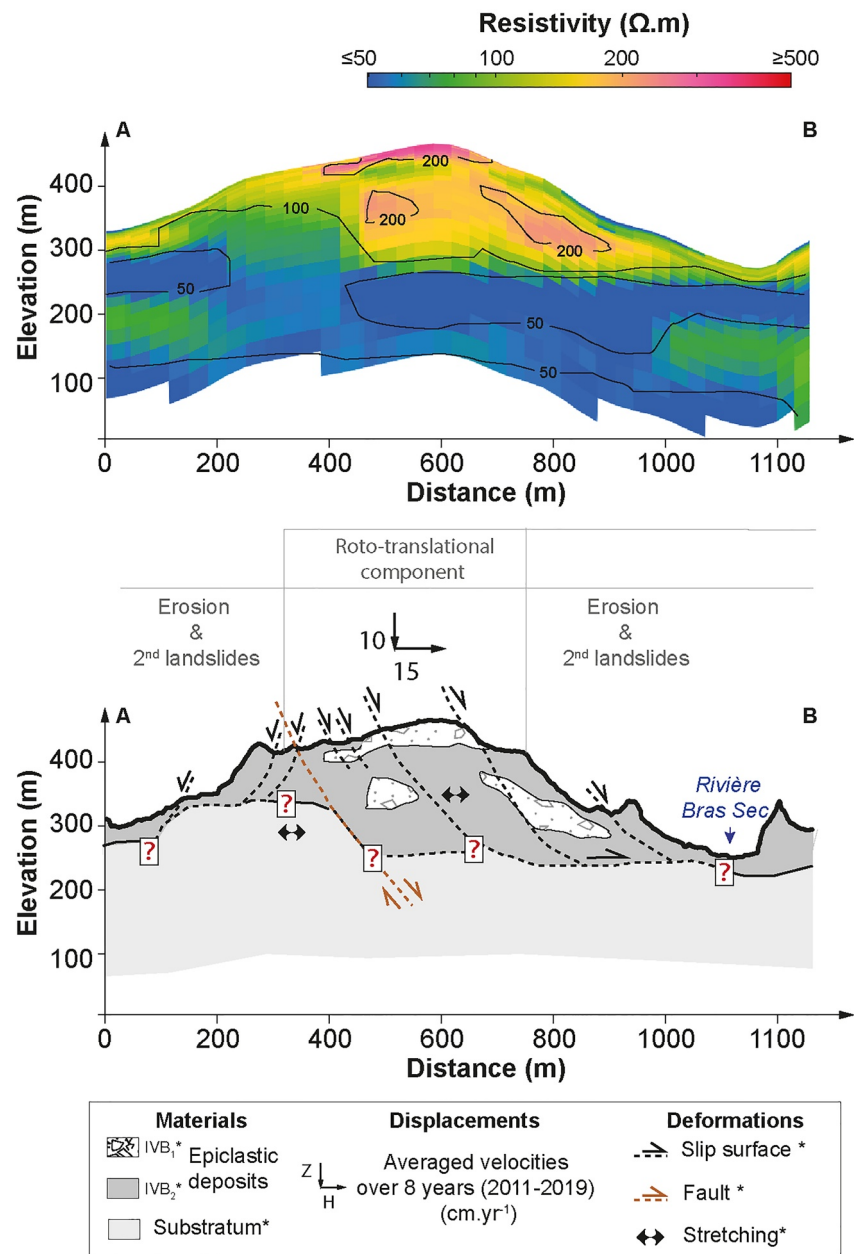
Figure 15. Interpretation of the internal structure of the Ilet à Vidot landslide along profile A–B shown in Figure 14. (a) Resistivity profile acquired by interpolation of the AEM data. The black lines are isoresistivity contours. (b) Conceptual morphodynamic cross-section of the landslide obtained using a compilation of the different data available (see Section 3). Symbol * means that the feature is deduced mainly from geophysical data. IVB1 and IVB2: facies of the Ilet à Vidot Breccia.

The western and eastern parts of the profile are separated by a large unconformity affecting the whole terrain imaged by AEM data. The vertical offset between the east and west resistive patches (>200 Ωm) along this unconformity suggests that it could correspond to a normal fault. The extension toward the surface of the other unconformities observed in the resistivity model coincides with the main scarps mapped, which can be construed as sliding surfaces. Using field observations, displacement measurements and the resistivity profile, it is assumed that the sliding surfaces drawn on profile A-B dip toward the rivers of the Bras Sec and Bras Fontaine east and west of the fault, respectively.

Therefore, taking into account their main sliding surface and their area, the volumes of the eastern and western landslides are c. 6.7×10^7 and 2×10^7 m^3, respectively.

Morphological features (e.g., scarps and cracks) and internal structures (sliding surfaces and faults) can indicate that the Ilet à Vidot Plateau is being eroded on both sides through rotational-translational landslides that are affected by second-order smaller landslides (e.g., DF triggered during rainstorms).

5. Discussion

5.1. An Atypical Environment Prone to Landslides

Volcaniclastic deposits derived from large-scale edifice failures are observed on many volcanoes worldwide (Holcomb & Searle, 1991; Van Wyk de Vries & Davies, 2015), for instance, on Stromboli (Italy, Apuani et al., 2005), Tahiti (Clément et al., 2003; Hildenbrand et al., 2008), Las Palmas (Canary Islands, Colmenero et al., 2012), Ischia Island (Italy, De Vita et al., 2006; Della Seta et al., 2012), Hawaii (Moore et al., 1989), Mt. Taranaki (New Zealand, Zernack, 2021), Mount St. Helens (Voight et al., 1983), and Flores Island (Hildenbrand et al., 2018). Some of these places display a high density of landslides (e.g., 19 landslides per km^2 on Flores Island (Portugal), Silva et al., 2018). Nevertheless, none of these locations nor other areas in Reunion Island present the density (about 10.7 landslides per km^2) and the diversity of Salazie's landslides. The combination of several factors, such as properties and structure of volcanoclastic deposits, climate, fluid circulation, and topography, can explain this exceptional diversity.

5.1.1. Epiclastic Deposits

In Salazie, epiclastic deposits mobilized by landslides comprise clasts with a wide range of sizes, shapes and volcanic lithologies (Arnaud, 2005; Haurie, 1987). This induces structural discontinuities and disparate mechanical properties, such as variation in porosity, cohesion, and angle of friction of the whole mass. Consequently, under intense rainfall, saturation and drainage conditions in these deposits may vary significantly through space and time, inducing increases in pore pressure and possible subsequent slope failures such as those triggered during Cyclone Hyacinthe along the lateral margins of the Grand Ilet plateau.

Furthermore, the epiclastic deposits contain various surfaces of weakness, such as shear zones within old debris deposits, between successive units, dikes, and faults (Arnaud, 2005; Chaput et al., 2017). Such surfaces can create geomechanical constraints favoring slope failure (Apuani et al., 2005; Crosta et al., 2005; Guzzetti et al., 2008; Jelínek & Wagner, 2007). For example, the bases of the Hell Bourg and Grand Ilet landslides coincide with unconformities in the epiclastic sequences and occur at the interface of two different lithological units (Arnaud, 2005; Belle, 2014; this study).

Discontinuities between materials with different mechanical behavior also favor the formation of shear surfaces within large sliding masses. Consequently, the landslide body might be divided into several sliding compartments with different kinematics, as observed in Grand Ilet, where tensile, compression and shear cracks result in morphological/structural features such as grabens or bulges, which are interpreted as a result of a velocity differential between the moving compartments.

Epiclastic deposits may also favor secondary sliding surfaces within the landslide, which is possibly the case in the north of the Hell Bourg landslide. Indeed, the resistivity contrasts within this landslide can be related to the original structure of the sliding debris-avalanche deposit. Large debris-avalanche deposits are known to contain megaclast-dominated portions interbedded with matrix-dominated portions and shear zones and slip surfaces developed at isolated and irregular locations within the flowing mass (e.g., Dufresne et al., 2021; Glicken, 1991; Roverato et al., 2015). In the resistivity profile of the Hell Bourg landslide, we interpret the high resistivity parts as possible megaclast-dominated portions and low resistivity as matrix-dominated portions. Fluid circulation at the interphase between these two facies, as assumed for the northern part of this landslide, could have created a slip surface and promoted a superficial landslide in this area.

5.1.2. Climate Conditions and Fluid Circulation

The maximum displacements are measured during the wet season, especially after intense rainfall. Belle et al. (2014) showed that the accelerations of the Hell Bourg and Grand Ilet landslides are controlled by variations in groundwater levels. Rapid and slow variations in the level of the water table due to infiltration through open fractures and in porous media explain the dynamics of landslide displacements in response to cyclonic rainstorms (Belle et al., 2014; Iverson, 2000).

The saturation of the terrain during Cyclone Hyacinthe reached the maximum described in the last 50 years due to exceptional precipitation amounts (Rault et al., 2022). Ponds were filled or overflowed, and many streams appeared on the îlets (Advenier & Stieltjes, 1990; Humbert et al., 1981). The pore pressure at the head of steep slopes was extremely high, exceeding the equilibrium threshold and thus leading the borders of the îlet to collapse, generating DF. The role of closed depressions as preferential zones of infiltration in maintaining high pore pressure and thus favoring landslide activity has been assumed but not yet fully proven (Advenier & Stieltjes, 1990). This has been suggested in particular for the landslides triggered during Cyclone Hyacinthe, as many filled, closed depressions were observed 100 m above the location of landslide heads (Pinchinot, 1984).

Moreover, ground fluid circulation may induce internal erosion processes such as suffosion (i.e., change in the porosity and mechanical properties of the terrain caused by the migration of fine particles within the epiclastic material due to water infiltration) that could be at least partially responsible for slope deformation and failure (Fannin & Moffat, 2006). Internal erosion is assumed to play a significant role in the formation of *déboulés* (Pinchinot, 1984). In 1991, small pipes with diameters of 1–5 cm were visible in the source area of a debris-flow formed during heavy rainfalls in the entrance of Salazie, in non-cohesive epiclastic deposits. These pipes are typical of internal erosion processes involved in gully formation and embankment collapses (Kirkby & Bracken, 2009). Internal erosion processes are also known to be involved in the formation of lavakas, as described by Riquier (1954) in Madagascar, that is, gullies formed in poorly cohesive material that show morphological similarities to the Ravine de l'Eglise.

On a larger time scale, hydrothermal and groundwater circulation also contributes to the instability of the terrain, reducing its strength by weathering (Moon et al., 2005; Shuzui, 2001; Swanson & Swanston, 1977). This process is supposed to occur at the base of the Grand Ilet and Hell Bourg landslides. Groundwater and hydrothermal circulation are identified at Grand Ilet and Hell Bourg (Belle, 2014; Bénard et al., 2020). There, water circulation along clay layers, resulting from the alteration of epiclastic material, reduces strength and leads to the forming of a "soap layer" (Arnaud, 2005; Belle, 2014).

All three *cirques* of Reunion Island are characterized by thick sequences of epiclastic deposit and have an irregular topography with steep slopes along the river valleys and cliffs. However, landslide activity in the *cirques* of Cilaos and Mafate is much lower than observed in Salazie (Humbert et al., 1981). There is little evidence of deformation in the inhabited areas, and the geodetic markers emplaced on the îlets do not record significant displacements (Mazué et al., 2013). In Mafate and Cilaos, the annual climate is drier than in Salazie. For example, between 1981 and 2010, there was an average of 42 and 91 days of precipitation in Mafate and Cilaos, respectively, which represented an average annual precipitation of 579 and 1,852 mm. During the same period, the Cirque de Salazie recorded an average of 137 rainy days per year and an average annual precipitation of 2,519 mm (cf. http://www.meteofrance.re). These drier climatic conditions are conducive neither to the formation of perennial water tables nor to the maintenance of large-scale landslide activity controlled by groundwater (Belle, 2014).

5.2. Successive Generations of Landslide Process: Toward a Conceptualization of the Dynamics of Volcano Edifice Dismantling

The most recent landslides in the Cirque de Salazie are the result of successive generations of slope movement. They remobilized epiclastic deposits derived from ancient large-scale flank failures of PN, some of which have already been reworked by historical landslides or are still active (Haurie, 1987). With each generation of landslides, the material is subject to various deformation processes and is therefore marked by a specific internal organization. To a lesser or greater degree, the next generation of landslides, which remobilize the former collapse deposits, inherits this organization and can itself be remobilized by younger landslides (Devoli et al., 2009).

Similarities can be observed between the original volcanic debris-avalanches deposits and the subsequent landslides that remobilize them (Arnaud, 2005; Bernard et al., 2009; Thompson et al., 2010). In Salazie, these similarities concern the internal and surficial morphological features of large compound landslides as well as the direction of their displacement (Oehler et al., 2004; Perinotto, 2014; this study). Internal and external factors might have caused the reactivation of these deposits, such as changes in fluid circulation within the deposits, downcutting incisions or even regional earthquakes (Bernard et al., 2009).

Recent landslides are also commonly observed in areas where older, now inactive landslides are identified (Samia et al., 2017). This is the case, for example, on îlets where we observe successive stable plateaus with arc-shaped

morphologies and a smaller active plateau in the lower part. Active compound landslides form complex moving terrains, where a variety of landslide and erosion processes interact to produce self-maintaining activity. Erosion processes and sudden landslides are often concentrated along steep slopes of the host landslide's toe and scarps, where non-cohesive epiclastic material crops out. This unstable material might be pushed downslope and sheared due to the ongoing displacement of the landslide, thus triggering secondary landslides (Cronin, 1992; Migoń et al., 2010; Swanson & Swanston, 1977). By removing considerable mass at the landslide toe downstream, these secondary landslides may reduce the stability of the host landslide and maintain its sensitivity to groundwater level fluctuation (Ferrari et al., 2011) and therefore its unstable regime.

5.3. Rainfall-Triggered Landslides and Volcano Dismantling

Landslides through space and time in the Cirque de Salazie illustrate the impact such events in volcano dismantling, a role that has been accentuated by the tropical climate in the case of Reunion Island (Gayer et al., 2019) or for example, Guadeloupe (Allemand et al., 2014) and Hawaii Island (Ferrier et al., 2013).

The erosion rate from landslide activity can be calculated by assuming a characteristic triggering event for the region that is repeated at regular intervals with the same total volume of landslides. Therefore, the average annual erosion rate can be estimated by determining the cumulative volume of material removed by landslides over a known area by this event and dividing this by the return period of the event (Malamud et al., 2004).

The Rivière du Mât is considered to be a torrential river with a wide grain-size range. Stollsteiner et al. (2008) evaluated its annual sediment transport capacity. To do so, they measured transversal profiles of the river to assess its grain-size range and morphological characteristics. They then used these characteristics to calculate the maximum annual transport capacity using a bed load equation (Sogreah-Lefort, Lefort, 1994) applied to flood hydrographs. The river discharge was measured from 2000 to 2007. The discharge before 2000 was estimated using a relationship between rainfall and river discharge. They obtained a good consistency between the transport capacity they had calculated and the volume of sediments they had estimated from DSM comparison. They showed that the annual sediment transport capacity of the Rivière du Mât averages 130,000 m^3 upstream and 1.2×10^6 to 1.6×10^6 m^3 downstream. The latter is therefore high; it can be even higher, reaching 1.5×10^6 m^3 upstream to 1.8×10^6 m^3 downstream during exceptional cyclonic rainstorms (Stollsteiner et al., 2008).

Considering that Cyclone Hyacinthe, which produced 10 days of heavy rainfall, has a return period of 100 years (Pinchinot, 1984), we infer that centennial events should produce an approximately equivalent volume of landslides ($V = 15.2 \pm 0.44 \times 10^6$ m^3). Scaled to the surface studied (121 km^2) and assuming in addition that all this volume will progressively be exported out of the cirque by the Rivière du Mât over a century (which seems a reasonable assumption considering the river's measured high transport capacity), the upper bound of the erosion rate due to landslides at Salazie is 1.13 ± 0.2 mm yr^{-1}.

This rate represents almost 20% of the long-term erosion rates of the Cirque de Salazie estimated by Gayer et al. (2019) for over 72 ka (7.4 mm yr^{-1}). Furthermore, our estimated erosion rate is also 5–10 times higher than the erosion rate produced by shallow landslides (2.7×10^{-2} to 4×10^{-2} mm yr^{-1}) calculated by Ferrier et al. (2013) in the Hanalei basin on the Hawaiian island of Kaua'i over a short period (<10 years) without any extreme events. Events occurring during the period over which erosion rate are calculated seem to influence the final estimate. The longer the period considered in the long-term erosion calculation is, the more likely extreme and rare events and their associated high erosion rates are integrated. Exceptional collapses (with return periods greater than 100-years), such as Grand Sable (18×10^6 m^3, 1875) or Mahavel (50×10^6 m^3, 1965) (Merle et al., 2008), also contribute to the island's long-term erosion (Garcin et al., 2005; Gayer et al., 2019; Kieffer, 1989). The return period of such events, and therefore their contribution to erosion, is difficult to assess due to their low frequency. Using our geomorphological approach, we are able to provide an initial assessment in quantifying the impact of landslides caused by a 100-year rainfall event on volcanic edifice degradation in the Cirque de Salazie. However, more complete inventories (e.g., longer time-scale and higher space scale [all Reunion Island]) would be required to better quantify the volume-frequency relation of the landslides and relate it to the dynamic of long-term erosion.

Table 3
Contribution of Innovative Methods Used in This Study for Hazard and Risk Analysis

Method	Most revealing information	Associated landslide	Relevance of the data for		
			Landslide process analysis	Landslide hazard analysis	Early warning
AEM	Type and depth of materials	Large landslides	++	+	−
	Slip surface of landslides		++	+	−
	Internal structure (3D, volume involved)		++	−	−
SFM-MVS	Morphology	Rapid landslides	++	++	−
	Landslide shape		++	++	++
	Historical information (frequency of landslide)		++	++	++
Lidar	Dynamic of landslides	All landslides	+	++	++
DEMs	Morphology		++	++	−

Note. Relevance level: ++ high, + medium, and − low.

5.4. Landslides and Hazard Assessment

Salazie illustrates the diversity of landslide processes that can occur in a volcanic environment dominated by epiclastic material. In this inhabited area, particular attention is given to landslide hazard and risk analyses, since such phenomena could cause high casualties and significant economic losses, as has occurred in the past (Cance & Rey, 2018).

Large flows can generate sudden significant regression of *îlet* borders or rock cliffs, cover large distances and potentially dam rivers. Occasionally, large RA like the one in Grand Sable occur in volcanic rocks, as observed in Hawaii (Jones et al., 1984) or the Philippines (Evans et al., 2007). Rapid and shallow landslides are frequent in volcaniclastic material, as observed on the Hawaiian, Azores, Vulcano and Ishia islands (e.g., Crosta et al., 2005; Deb & El-Kadi, 2009; Di Martire et al., 2012; Ferrucci et al., 2005; Valadão et al., 2002). Under very intense rainfall, *deboulé*, as observed in Grand Ilet, can induce the sudden formation of long, large gullies cutting into plateaus. These rapid processes have potentially catastrophic consequences, especially for inhabited areas, consequences that can be amplified by the sudden rupture of river dams. Moreover, the frequency of these processes may increase in response to a higher frequency of extreme rainstorms associated with climate change.

Large slow-moving landslides (compound and RtSs), which make up a significant proportion of the inhabited area, may accelerate rapidly, move over unusually large distances or fail suddenly due to changes in stress conditions, in addition to their regular movement (Lacroix et al., 2020). Such behavior may cause serious damage to infrastructure networks and housing, as observed in Salazie but also in other volcanic areas, such as the Western Carpathian (Prokešová et al., 2010), the Cascade Range (Swanson & Swanston, 1977) and the Hawaiian Islands (Baum & Reid, 1992).

At longer time scales, observations and discussions in this study support the idea that epiclastic deposits that currently appear stable might be remobilized in response to specific geological and climatic conditions. Change in climatic conditions at the scale of Reunion Island, might induce hydrological changes and cause activation of currently stable terrain. Further analyses and simulations are required to better understand the dynamics of the stabilization and reactivation of these deposits to provide input to discussions on hazards related to these loose epiclastic deposits.

This multidisciplinary study provides valuable insights into the geological, structural, hydrogeological and climatic parameters involved in landslide phenomena, along with a detailed description of the various typologies of landslides encountered in Salazie. This information is essential for landslide hazard assessments and risk mitigation (Corominas et al., 2014; Van Westen et al., 2008). This work also provides some additional information on the contribution of the different methods that can be used for developing a landslide risk analysis framework (advantages, disadvantages, costs, scale of work, and applications) (Table 3). From the methods used in this study, the innovations listed below can easily be replicated in other volcanic or non-volcanic environments to identify relevant information on landslide processes and areas prone to landslides:

1. AEM combined with geomorphological and geological observations allowed us to delineate three large landslides and define their internal structure. This method has also been successfully used on the volcanic island of Martinique (Thiery et al., 2017, 2021) and thus seems suitable for deep imaging of complex volcanic environments and identifying landslide-prone material. This information can then be used, for example, to elaborate landslide scenarios with deterministic models (Thiery et al., 2017, 2021).

2. SFM-MVS applied on historical aerial photographs allowed the production of pre- and post-cyclone event images and DEM of irregular and steep topography. Using these data, we delineated rain-triggered landslides and quantified their volume. This method is promising and provides essential information for landslide hazard mitigation mapping (Gomez et al., 2015; Riquelme et al., 2019; Rault et al., 2020, 2022). For example, it has provided quantitative information on a 100-year rainfall event in this study.

3. The comparison of high-resolution lidar DEMs provided integrated information on morphological changes due to fast and slow landslides (Booth et al., 2018; James et al., 2012). It also provides information on the spatial dynamics of landslides.

6. Conclusions

The rapid erosion of volcanic edifices and the formation of deeply incised valleys are often attributed to massive collapses of the volcanic flanks. However, other smaller but more frequent slope failures also contribute to the degradation of edifices. The Cirque de Salazie is an example of a young funnel-shaped valley resulting from successive failures of the flanks of the volcanic edifice. Mass movements still participate actively in the *cirque*'s morphological evolution and directly threaten the local population.

In this study, we combined 50 years of knowledge of Salazie's landslides with field observations and new technical approaches to characterize landslide activity and processes at the scale of the *cirque*.

We showed that at least 19% of the *cirque* area is affected by landslides, more than 57% of which have recently been active. Most of landslides remobilized epiclastic deposits coming from previous volcano flank collapses.

Landslide processes in Salazie are remarkable due to their size and mechanisms. These particularities are mainly explained by the interplay of the multiphase history of the materials involved and the tropical climate characterized by high annual rainfall and intense rainstorms. It was necessary to define a typology adapted to this environment and to provide a detailed description of the landslides to better understand their origin, processes and role in the erosion of the volcanic edifice. Taking into account criteria characterizing the material, the hydrodynamic context of failure, the geometry, the displacement rate and run-out, we defined and characterized eight types of landslides occurring in this volcanic environment. Among them, three compound landslides represent some of the largest inhabited slow-moving landslides identified worldwide. These three landslides have their own complex structure and dynamics, which are linked to the history of the remobilized epiclastic material, together with the complex hydrogeological network and the secondary landslides and erosion processes.

Our results also suggest that landslides triggered by a 100-year cyclone rainstorm prepare a high volume of material to be evacuated out of the *cirque* over a century. This volume could contribute to almost 20% of the long-term erosion rate of the volcanic edifice. Erosion by landslides in the Cirque de Salazie is particularly intense due to the combination of favorable climatic, orographic and geologic conditions, but is also boosted by the self-reinforcing activity of erosion and landslide processes. These conditions are rarely fulfilled even at the scale of the island, thus making Salazie an area that is exceptionally prone to landslides.

The study of Salazie's landslides offers quantifiable elements for understanding the sliding mechanisms in the dismantling of volcanic edifice over large timescales. Through their activity, density and diversity, the landslides of this open-air laboratory provide key information for landslide hazard assessment in volcanic and non-volcanic regions. This study also offers new insights for research on the role of landslides in the dissection of volcanic edifices.

Data Availability Statement

Most of the data are available through reports and articles listed in Table 1. The landslide shapefile is available in the following repository https://data.mendeley.com/datasets/gvkjpp87xj/3. Archive aerial photographs are available for free at https://remonterletemps.ign.fr/. AEM surveys are available through Martelet et al. (2014).

References

Advenier, P., & Stieltjes, L. (1990). *Etude du drainage du plateau de Grand Ilet* (No. 90Reu34). BRGM.

Allemand, P., Delacourt, C., Lajeunesse, E., Devauchelle, O., & Beauducel, F. (2014). Erosive effects of the storm Helena (1963) on Basse Terre Island (Guadeloupe—Lesser Antilles Arc). *Geomorphology*, *206*, 79–86. https://doi.org/10.1016/j.geomorph.2013.09.020

Apuani, T., Corazzato, C., Cancelli, A., & Tibaldi, A. (2005). Stability of a collapsing volcano (Stromboli, Italy): Limit equilibrium analysis and numerical modelling. *Journal of Volcanology and Geothermal Research*, *144*(1–4), 191–210. https://doi.org/10.1016/j.jvolgeores.2004.11.028

Arnaud, N. (2005). *Les processus de démantèlement des volcans, le cas d'un volcan bouclier en milieu océanique: Le Piton des Neiges, Île de la Réunion (Sciences de la Terre)*. Université de la Réunion. Retrieved from http://www.theses.fr/2005LARE0011

Aunay, B., & Rey, A. (2018). *Cirque de Salazie: Exposition des habitations aux phénomènes gravitaires Compléments d'information du rapport Aunay (2015)* (No. RP-67984-FR, p. 17). BRGM. Retrieved from http://infoterre.brgm.fr/rapports/RP-67984-FR.pdf

Baltassat, J. M., Roulle, A., Bitri, A., & Aunay, B. (2016). *Investigations géophysiques du secteur de Grand Ilet (Salazie)* (No. RP-61360-FR, p. 58). BRGM. Retrieved from http://infoterre.brgm.fr/rapports/RP-61360-FR.pdf

Barbano, M. S., Pappalardo, G., Pirrotta, C., & Mineo, S. (2014). Landslide triggers along volcanic rock slopes in eastern Sicily (Italy). *Natural Hazards*, *73*(3), 1587–1607. https://doi.org/10.1007/s11069-014-1160-1

Barbary, D., Leroux, M. D., & Bousquet, O. (2019). The orographic effect of La Réunion Island on tropical cyclone track and intensity. *Atmospheric Science Letters*, *20*(2), 9. https://doi.org/10.1002/asl.882

Barcelo, A., & Coudray, J. (1996). Nouvelle carte des isohyètes annuelles et des maxima pluviométriques sur le massif du Piton de la Fournaise (Ile de la Réunion). *Revue des Sciences de l'Eau*, *29*.

Barcelo, A., Robert, R., & Coudray, J. (1997). A major rainfall event: The 27 February–5 March 1993 rains on the southeastern slope of Piton de la Fournaise Massif (La Réunion Island, Southwest Indian Ocean). *Monthly Weather Review*, *125*, 6.

Baum, R. L., & Reid, M. E. (1992). *Geology, hydrology and mechanics of the Alani-Paty Landslide, Manoa Valley, Oahu, Hawaii* (Report No. 92–501). https://doi.org/10.3133/ofr92501

Bellanger, A., & Aunay, B. (2008). *Suivi des glissements d'Hell-Bourg et de Grand Ilet par les stations GPS permanentes* (No. RP-56708-FR, p. 64). BRGM. Retrieved from http://ficheinfoterre.brgm.fr/document/RP-56708-FR

Belle, P (2014). Contribution des processus hydrologiques et hydrogéologiques aux glissements de terrain de grande ampleur : application au contexte tropical de la Réunion. Géologie appliquée. Université de la Réunion. Français. Retrieved from https://tel.archives-ouvertes.fr/tel-01155266

Belle, P., Aunay, B., Bernardie, S., Grandjean, G., Ladouche, B., Mazué, R., & Join, J. L. (2014). The application of an innovative inverse model for understanding and predicting landslide movements (Salazie cirque landslides, La Réunion Island). *Landslides*, *11*(3), 343–355. https://doi.org/10.1007/s10346-013-0393-5

Belle, P., Aunay, B., Lachassagne, P., Ladouche, B., & Join, J. L. (2018). Control of tropical landcover and soil properties on landslides' aquifer recharge, piezometry and dynamics. *Water*, *10*(10), 1491. https://doi.org/10.3390/w10101491

Bénard, B., Famin, V., Agrinier, P., Aunay, B., Lebeau, G., Sanjuan, B., et al. (2020). Origin and fate of hydrothermal fluids at Piton des Neiges volcano (Réunion Island): A geochemical and isotopic (O, H, C, Sr, Li, Cl) study of thermal springs. *Journal of Volcanology and Geothermal Research*, *392*, 106682. https://doi.org/10.1016/j.jvolgeores.2019.106682

Bernard, B., Takarada, S., Andrade, D. A., & Dufresne, A. (2021). Terminology and strategy to describe large volcanic landslides and Debris Avalanches. In *Volcanic Debris Avalanches, An Official Book Series of the International Association of Volcanology and Chemistry of the Earth's Interior* (pp. 51–73). Springer. https://doi.org/10.1007/978-3-030-57411-6_3

Bernard, B., van Wyk de Vries, B., & Leyrit, H. (2009). Distinguishing volcanic debris avalanche deposits from their reworked products: The Perrier sequence (French Massif Central). *Bulletin of Volcanology*, *71*(9), 1041–1056. https://doi.org/10.1007/s00445-009-0285-7

Berthod, C., Famin, V., Bascou, J., Michon, L., Ildefonse, B., & Monié, P. (2016). Evidence of sheared sills related to flank destabilization in a basaltic volcano. *Tectonophysics*, *674*, 195–209. https://doi.org/10.1016/j.tecto.2016.02.017

Blahůt, J., Balek, J., Klimeš, J., Rowberry, M., Kusák, M., & Kalina, J. (2019). A comprehensive global database of giant landslides on volcanic islands. *Landslides*, *16*(10), 2045–2052. https://doi.org/10.1007/s10346-019-01275-8

Blijenberg, H. (1998). *Rolling stones?: Triggering and frequency of hillslope debris flows in the Bachelard Valley, southern French Alps*. Netherlands Geographical Studies.

Booth, A. M., McCarley, J., Hinkle, J., Shaw, S., Ampuero, J.-P., & Lamb, M. P. (2018). Transient reactivation of a deep-seated landslide by undrained loading captured with repeat airborne and Terrestrial Lidar. *Geophysical Research Letters*, *45*(10), 4841–4850. https://doi.org/10.1029/2018GL077812

Borgia, A., Delaney, P. T., & Denlinger, R. P. (2000). Spreading volcanoes. *Annual Review of Earth and Planetary Sciences*, *28*(1), 539–570. https://doi.org/10.1146/annurev.earth.28.1.539

Bret, L., Fevre, Y., Join, J. L., Robineau, B., & Bachelery, P. (2003). Deposits related to degradation processes on Piton des Neiges Volcano (La Réunion Island): Overview and geological hazard. *Journal of Volcanology and Geothermal Research*, *123*(1–2), 25–41. https://doi.org/10.1016/S0377-0273(03)00026-X

Brideau, M.-A., & Roberts, N. J. (2015). Mass movement in bedrock. In *Landslide hazards, risks and disasters* (pp. 43–90). Elsevier. https://doi.org/10.1016/B978-0-12-396452-6.00003-3

Byrne, P. K., Holohan, E. P., Kervyn, M., van Wyk de Vries, B., Troll, V. R., & Murray, J. B. (2013). A sagging-spreading continuum of large volcano structure. *Geology*, *41*(3), 339–342. https://doi.org/10.1130/G33990.1

Calcaterra, D., Coppin, D., de Vita, S., Di Vito, M. A., Orsi, G., Palma, B., & Parise, M. (2007). Slope processes in weathered volcaniclastic deposits within the city of Naples: The Camaldoli Hill case. *Geomorphology*, *87*(3), 132–157. https://doi.org/10.1016/j.geomorph.2006.03.040

Cance, A., & Rey, A. (2018). *Suivi du réseau géodésique du cirque de Salazie* (p. 40). BRGM.

Carracedo, J. C., Day, S. J., Guillou, H., & Pérez Torrado, F. J. (1999). Giant Quaternary landslides in the evolution of La Palma and El Hierro, Canary Islands. *Journal of Volcanology and Geothermal Research*, *94*(1–4), 169–190. https://doi.org/10.1016/S0377-0273(99)00102-X

Cas, R. A. F., & Wright, J. V. (1988). Epiclastic processes in volcanic terrains. In *Volcanic successions modern and ancient* (pp. 292–330). Springer.

Chaggar, T. S. (1984). La Réunion sets new rainfall records. *Weather*, *31*(1), 12–14. https://doi.org/10.1002/j.1477-8696.1984.tb05440.x

Chaput, M. (2013). *Déformation et activité intrusive des volcans boucliers – Du terrain à la modélisation numérique (Piton des Neiges, La Réunion)*. Université de la Réunion. Retrieved from https://tel.archives-ouvertes.fr/tel-00967104

Chaput, M., Famin, V., & Michon, L. (2014). Deformation of basaltic shield volcanoes under cointrusive stress permutations. *Journal of Geophysical Research: Solid Earth*, *119*(1), 1195–1209. https://doi.org/10.1002/2013JB010623

Chaput, M., Famin, V., & Michon, L. (2017). Sheet intrusions and deformation of Piton des Neiges, and their implication for the volcano-tectonics of La Réunion. *Tectonophysics*, *717*, 531–546. https://doi.org/10.1016/j.tecto.2017.08.039

Clément, J.-P., Legendre, C., Caroff, M., Guillou, H., Cotten, J., Bollinger, C., & Guille, G. (2003). Epiclastic deposits and 'horseshoe-shaped' calderas in Tahiti (Society Islands) and Ua Huka (Marquesas Archipelago), French Polynesia. *Journal of Volcanology and Geothermal Research*, *120*(1), 87–101. https://doi.org/10.1016/S0377-0273(02)00366-9

Colmenero, J. R., de la Nuez, J., Casillas, R., & Castillo, C. (2012). Epiclastic deposits associated with large-scale landslides and the formation of erosive calderas in oceanic islands: The example of the La Palma Island (Canary Archipelago). *Geomorphology*, *177–178*, 108–127. https://doi.org/10.1016/j.geomorph.2012.07.019

Corominas, J., van Westen, C., Frattini, P., Cascini, L., Malet, J.-P., Fotopoulou, S., et al. (2014). Recommendations for the quantitative analysis of landslide risk. *Bulletin of Engineering Geology and the Environment*, *73*(2), 209–263. https://doi.org/10.1007/s10064-013-0538-8

Costa, J. E. (1984). Physical geomorphology of debris flows. In *Developments and applications in geomorphology* (pp. 268–317). Springer Verlag. https://doi.org/10.1007/978-3-642-69759-3_9

Cronin, V. S. (1992). Compound landslides: Nature and hazard potential of secondary landslides within host landslides. In J. E. Slosson, A. G. Keene, & J. A. Johnson (Eds.), *Landslides/Landslide Mitigation* (Vol. 9). Geological Society of America. https://doi.org/10.1130/REG9-p1

Crosta, G. B., Hermanns, R. L., Dehls, J., Lari, S., & Sepulveda, S. (2017). Rock avalanches clusters along the northern Chile coastal scarp. *Geomorphology*, *289*, 27–43. https://doi.org/10.1016/j.geomorph.2016.11.024

Crosta, G. B., Imposimato, S., Roddeman, D., Chiesa, S., & Moia, F. (2005). Small fast-moving flow-like landslides in volcanic deposits: The 2001 Las Colinas Landslide (El Salvador). *Engineering Geology*, *79*(3–4), 185–214. https://doi.org/10.1016/j.enggeo.2005.01.014

Cruden, D. M., & Varnes, D. J. (1996). *Landslides: Investigation and mitigation. Chapter 3-Landslide types and processes* (Transportation Research Board Special Report No. 247). ISSN: 0360-859X.

Deb, S. K., & El-Kadi, A. I. (2009). Susceptibility assessment of shallow landslides on Oahu, Hawaii, under extreme-rainfall events. *Geomorphology*, *108*(3), 219–233. https://doi.org/10.1016/j.geomorph.2009.01.009

Delcamp, A., van Wyk de Vries, B., & James, M. R. (2008). The influence of edifice slope and substrata on volcano spreading. *Journal of Volcanology and Geothermal Research*, *177*(4), 925–943. https://doi.org/10.1016/j.jvolgeores.2008.07.014

Delcamp, A., van Wyk de Vries, B., James, M. R., Gailler, L. S., & Lebas, E. (2012). Relationships between volcano gravitational spreading and magma intrusion. *Bulletin of Volcanology*, *74*(3), 743–765. https://doi.org/10.1007/s00445-011-0558-9

Della Seta, M., Marotta, E., Orsi, G., de Vita, S., Sansivero, F., & Fredi, P. (2012). Slope instability induced by volcano-tectonics as an additional source of hazard in active volcanic areas: The case of Ischia Island (Italy). *Bulletin of Volcanology*, *74*(1), 79–106. https://doi.org/10.1007/s00445-011-0501-0

Del Potro, R., & Hürlimann, M. (2008). Geotechnical classification and characterisation of materials for stability analyses of large volcanic slopes. *Engineering Geology*, *98*(1–2), 1–17. https://doi.org/10.1016/j.enggeo.2007.11.007

De Vita, S., Sansivero, F., Orsi, G., & Marotta, E. (2006). Cyclical slope instability and volcanism related to volcano-tectonism in resurgent calderas: The Ischia Island (Italy) case study. *Engineering Geology*, *86*(2–3), 148–165. https://doi.org/10.1016/j.enggeo.2006.02.013

Devoli, G., De Blasio, F. V., Elverhøi, A., & Høeg, K. (2009). Statistical analysis of landslide events in Central America and their run-out distance. *Geotechnical & Geological Engineering*, *27*(1), 23–42. https://doi.org/10.1007/s10706-008-9209-0

Dikau, R., Brunsden, D., Schrott, L., & Ibsen, M. L. (1996). *Landslide recognition: Identification, movement, and causes*. Wiley.

Di Martire, D., De Rosa, M., Pesce, V., Santangelo, M. A., & Calcaterra, D. (2012). Landslide hazard and land management in high-density urban areas of Campania region, Italy. *Natural Hazards and Earth System Sciences*, *12*(4), 905–926. https://doi.org/10.5194/nhess-12-905-2012

Di Traglia, F., Bartolini, S., Artesi, E., Nolesini, T., Ciampalini, A., Lagomarsino, D., et al. (2018). Susceptibility of intrusion-related landslides at volcanic islands: The Stromboli case study. *Landslides*, *15*(1), 21–29. https://doi.org/10.1007/s10346-017-0866-z

Dou, J., Yunus, A. P., Tien Bui, D., Merghadi, A., Sahana, M., Zhu, Z., et al. (2019). Assessment of advanced random forest and decision tree algorithms for modeling rainfall-induced landslide susceptibility in the Izu-Oshima Volcanic Island, Japan. *The Science of the Total Environment*, *662*, 332–346. https://doi.org/10.1016/j.scitotenv.2019.01.221

Dufresne, A., Bösmeier, A., & Prager, C. (2016). Sedimentology of rock avalanche deposits – Case study and review. *Earth-Science Reviews*, *163*, 234–259. https://doi.org/10.1016/j.earscirev.2016.10.002

Dufresne, A., Siebert, L., & Bernard, B. (2021). Distribution and geometric parameters of volcanic debris avalanche deposits. In *Volcanic Debris Avalanches* (pp. 75–90). Springer. https://doi.org/10.1007/978-3-030-57411-6_4

Dumont, M., Peltier, A., Roblin, E., Reninger, P. A., Barde-Cabusson, S., Finizola, A., & Ferrazzini, V. (2019). Imagery of internal structure and destabilization features of active volcano by 3D high resolution airborne electromagnetism. *Scientific Reports*, *9*(1), 18280. https://doi.org/10.1038/s41598-019-54415-4

Dupond, J. F. (1984). Landslide and mudflow in young volcanic Hawaiian type structure. *Science of Tsunami Hazards*, *2*(1), 31–40.

Evans, S. G., Guthrie, R. H., Roberts, N. J., & Bishop, N. F. (2007). The disastrous 17 February 2006 rockslide-debris avalanche on Leyte Island, Philippines: A catastrophic landslide in tropical mountain terrain. *Natural Hazards and Earth System Sciences*, *7*(1), 89–101. https://doi.org/10.5194/nhess-7-89-2007

Famin, V., Berthod, C., Michon, L., Eychenne, J., Brothelande, E., Mahabot, M.-M., & Chaput, M. (2016). Localization of magma injections, hydrothermal alteration, and deformation in a volcanic detachment (Piton des Neiges, La Réunion). *Journal of Geodynamics*, *101*, 155–169. https://doi.org/10.1016/j.jog.2016.05.007

Famin, V., & Michon, L. (2010). Volcano destabilization by magma injections in a detachment. *Geology*, *38*(3), 219–222. https://doi.org/10.1130/G30717.1

Fannin, R. J., & Moffat, R. (2006). Observations on internal stability of cohesionless soils. *Géotechnique*, *56*(7), 497–500. https://doi.org/10.1680/geot.2006.56.7.497

Ferrari, A., Ledesma, A., González, D. A., & Corominas, J. (2011). Effects of the foot evolution on the behaviour of slow-moving landslides. *Engineering Geology*, *117*(3–4), 217–228. https://doi.org/10.1016/j.enggeo.2010.11.001

Ferrier, K. L., Perron, J. T., Mukhopadhyay, S., Rosener, M., Stock, J. D., Huppert, K. L., & Slosberg, M. (2013). Covariation of climate and long-term erosion rates across a steep rainfall gradient on the Hawaiian island of Kaua'i. *The Geological Society of America Bulletin*, *125*(7–8), 1146–1163. https://doi.org/10.1130/B30726.1

Ferrucci, M., Pertusati, S., Sulpizio, R., Zanchetta, G., Pareschi, M. T., & Santacroce, R. (2005). Volcaniclastic debris flows at La Fossa Volcano (Vulcano Island, southern Italy): Insights for erosion behaviour of loose pyroclastic material on steep slopes. *Journal of Volcanology and Geothermal Research*, *145*(3), 173–191. https://doi.org/10.1016/j.jvolgeores.2005.01.013

Flageollet, J.-C. (1996). The time dimension in the study of mass movement. *Geomorphology*, *15*(3-4), 185–190. https://doi.org/10.1016/0169-555x(95)00069-h

Gailler, L. S., & Lénat, J. F. (2012). Internal architecture of La Réunion (Indian Ocean) inferred from geophysical data. *Journal of Volcanology and Geothermal Research*, *221*, 83–98. https://doi.org/10.1016/j.jvolgeores.2012.01.015

Garcin, M., Poisson, B., & Pouget, R. (2005). High rates of geomorphological processes in a tropical area: The Remparts river case study (Réunion Island, Indian Ocean). *Geomorphology*, *67*(3–4), 335–350. https://doi.org/10.1016/j.geomorph.2004.11.002

Gayer, E., Michon, L., Louvat, P., & Gaillardet, J. (2019). Storm-induced precipitation variability control of long-term erosion. *Earth and Planetary Science Letters*, *517*, 61–70. https://doi.org/10.1016/j.epsl.2019.04.003

Gayer, E., Michon, L., & Villeneuve, N. (2021). Volcanic island multi-stage construction inferred from a simple geometrical approach: Example of Réunion Island. *Geomorphology*, *392*, 107900. https://doi.org/10.1016/j.geomorph.2021.107900

Glicken, H. (1991). Sedimentary architecture of large volcanic-Debris Avalanches. In R. V. Fisher & G. A. Smith (Eds.), *Sedimentation in Volcanic Settings* (Vol. 45). SEPM Society for Sedimentary Geology. https://doi.org/10.2110/pec.91.45.0099

Godio, A., & Bottino, G. (2001). Electrical and electromagnetic investigation for landslide characterisation. *Physics and Chemistry of the Earth – Part C: Solar, Terrestrial & Planetary Science*, *26*(9), 705–710. https://doi.org/10.1016/S1464-1917(01)00070-8

Gomez, C., Hayakawa, Y., & Obanawa, H. (2015). A study of Japanese landscapes using structure from motion derived DSMs and DEMs based on historical aerial photographs: New opportunities for vegetation monitoring and diachronic geomorphology. *Geomorphology*, *242*, 11–20. https://doi.org/10.1016/j.geomorph.2015.02.021

Guzzetti, F., Peruccacci, S., Rossi, M., & Stark, C. P. (2008). The rainfall intensity-duration control of shallow landslides and debris flows: An update. *Landslides*, *5*(1), 3–17. https://doi.org/10.1007/s10346-007-0112-1

Haurie, J. L. (1987). *Géodynamique des cirques de la Réunion: Implications géotechniques et stabilité des versants*. Université Scientifique et Médicale de Grenoble.

Hibert, C., Mangeney, A., Grandjean, G., & Shapiro, N. M. (2011). Slope instabilities in Dolomieu crater, Réunion Island: From seismic signals to rockfall characteristics. *Journal of Geophysical Research*, *116*(F4), F04032. https://doi.org/10.1029/2011JF002038

Hildenbrand, A., Gillot, P.-Y., & Marlin, C. (2008). Geomorphological study of long-term erosion on a tropical volcanic ocean island: Tahiti-Nui (French Polynesia). *Geomorphology*, *93*(3–4), 460–481. https://doi.org/10.1016/j.geomorph.2007.03.012

Hildenbrand, A., Marques, F. O., & Catalão, J. (2018). Large-scale mass wasting on small volcanic islands revealed by the study of Flores Island (Azores). *Scientific Reports*, *8*(1), 13898. https://doi.org/10.1038/s41598-018-32253-0

Holcomb, R. T., & Searle, R. C. (1991). Large landslides from oceanic volcanoes. *Marine Georesources & Geotechnology*, *10*(1–2), 19–32. https://doi.org/10.1080/10641199109379880

Humbert, M., Pasquet, R., & Stieljes, L. (1981). *Les risques géologiques dans les cirques de Salazie et de Cilaos (Ile de la Réunion)* (No. 81SNG543, p. 97). BRGM. Retrieved from http://infoterre.brgm.fr/rapports/81-SGN-543-GEG.pdf

Hungr, O., & Evans, S. G. (2004). Entrainment of debris in rock avalanches: An analysis of a long run-out mechanism. *The Geological Society of America Bulletin*, *116*(9–10), 1240–1252. https://doi.org/10.1130/B25362.1

Hungr, O., Evans, S. G., Bovis, M. J., & Hutchinson, J. N. (2001). Review of the classification of landslides of the flow type. *Environmental and Engineering Geoscience*, *7*(3), 221–238. https://doi.org/10.2113/gseegeosci.7.3.221

Hungr, O., Leroueil, S., & Picarelli, L. (2014). The Varnes classification of landslide types, an update. *Landslides*, *11*(2), 167–194. https://doi.org/10.1007/s10346-013-0436-y

Iverson, R. M. (2000). Landslide triggering by rain infiltration. *Water Resources Research*, *36*(7), 1897–1910. https://doi.org/10.1029/2000WR900090

Iverson, R. M., Reid, M. E., & LaHusen, R. G. (1997). Debris-flow mobilization from landslides. *Annual Review of Earth and Planetary Sciences*, *25*(1), 85–138. https://doi.org/10.1146/annurev.earth.25.1.85

James, L. A., Hodgson, M. E., Ghoshal, S., & Latiolais, M. M. (2012). Geomorphic change detection using historic maps and DEM differencing: The temporal dimension of geospatial analysis. *Geomorphology*, *137*(1), 181–198. https://doi.org/10.1016/j.geomorph.2010.10.039

Jelínek, R., & Wagner, P. (2007). Landslide hazard zonation by deterministic analysis (Veľká Čausa landslide area, Slovakia). *Landslides*, *4*(4), 339–350. https://doi.org/10.1007/s10346-007-0089-9

Johnson, A. M., & Rodine, J. D. (1984). Debris flow. In D. Brunsden & D. D. Prior (Eds.), *Slope instability* (pp. 257–361). John Wiley and Sons.

Jones, B. L., Chinn, S. S. W., & Brice, J. C. (1984). Olokele rock avalanche, island of Kauai, Hawaii. *Geology*, *12*(4), 209–211. https://doi.org/10.1130/0091-7613(1984)12<209:oraiok>2.0.co;2

Karátson, D., Thouret, J.-C., Moriya, I., & Lomoschitz, A. (1999). Erosion calderas: Origins, processes, structural and climatic control. *Bulletin of Volcanology*, *61*(3), 174–193. https://doi.org/10.1007/s004450050270

Kieffer, G. (1989). La formation des cirques du massif du Piton des Neiges (Ile de la Réunion). *Bulletin de la l'association géographique française*, *5*(66), 361–370. https://doi.org/10.3406/bagf.1989.1502

Kirkby, M., & Bracken, L. (2009). Gully processes and gully dynamics. *Earth Surface Processes and Landforms: The Journal of the British Geomorphological Research Group*, *34*(14), 1841–1851. https://doi.org/10.1002/esp.1866

Lacquement, F., & Nehlig, P. (2008). *Notice des cartes géologiques du Piton des Neiges (Ile de La Réunion, France)* (No. RP-56730-FR, p. 96). Retrieved from http://infoterre.brgm.fr/rapports/RP-56730-FR.pdf

Lacroix, P., Handwerger, A. L., & Bièvre, G. (2020). Life and death of slow-moving landslides. *Nature Reviews Earth & Environment*, *17*(8), 404–419. https://doi.org/10.1038/s43017-020-0072-8

Larsen, I. J., Montgomery, D. R., & Korup, O. (2010). Landslide erosion controlled by hillslope material. *Nature Geoscience*, *3*(4), 247–251. https://doi.org/10.1038/ngeo776

Lefort, P. (1994). *Autoroute de Maurienne. Aménagement du site de l'Echaillon* (p. 13). SFTRF.

Legros, F. (2002). The mobility of long-runout landslides. *Engineering Geology*, *63*(3–4), 301–331. https://doi.org/10.1016/S0013-7952(01)00090-4

Louvat, P., & Allègre, C. J. (1997). Present denudation rates on the island of Réunion determined by river geochemistry: Basalt weathering and mass budget between chemical and mechanical erosions. *Geochimica et Cosmochimica Acta*, *61*(17), 3645–3669. https://doi.org/10.1016/S0016-7037(97)00180-4

Lustremant, D. (1981). *L'éboulement d'extension catastrophique de Grand Sable, cirque de Salazie (île de la réunion, Océan Indien)* (No. 81REU05) (p. 7). BRGM.

Major, J. J., Pierson, T. C., & Scott, K. M. (2005). Debris flows at Mount St. Helens, Washington, USA. In M. Jakob & O. Hungr (Eds.), *Debris-flow hazards and related phenomena* (pp. 685–731). Springer Berlin Heidelberg. https://doi.org/10.1007/3-540-27129-5_27

Malamud, B. D., Turcotte, D. L., Guzzetti, F., & Reichenbach, P. (2004). Landslides, earthquakes, and erosion. *Earth and Planetary Science Letters*, *229*(1–2), 45–59. https://doi.org/10.1016/j.epsl.2004.10.018

Marc, O., & Hovius, N. (2015). Amalgamation in landslide maps: Effects and automatic detection. *Natural Hazards and Earth System Sciences*, *15*(4), 723–733. https://doi.org/10.5194/nhess-15-723-2015

Martelet, G., Reninger, P. A., Perrin, J., & Deparis, J. (2014). *Acquisition géophysique héliportée de l'île de La Réunion* (No. RP-63818-FR). BRGM. Retrieved from https://infoterre.brgm.fr/rapports/RP-63818-FR.pdf

Martí, J., Hurlimann, M., Ablay, G. J., & Gudmundsson, A. (1997). Vertical and lateral collapses on Tenerife (Canary Islands) and other volcanic ocean islands. *Geology*, *25*(10), 879–882. https://doi.org/10.1130/0091-7613

Masson, D. G. (1996). Catastrophic collapse of the volcanic island of Hierro 15 ka ago and the history of landslides in the Canary Islands. *Geology*, *24*(3), 231–234. https://doi.org/10.1130/0091-7613

Mather, A. E., Griffiths, J. S., & Stokes, M. (2003). Anatomy of a 'fossil' landslide from the Pleistocene of SE Spain. *Geomorphology*, *50*(1–3), 135–149. https://doi.org/10.1016/S0169-555X(02)00211-8

Mazué, R., Aunay, B., & Belle, P. (2013). *Suivi des réseaux géodésiques dans les cirques de La Réunion* (No. RP-61994-FR) (p. 66). BRGM. Retrieved from http://infoterre.brgm.fr/rapports/RP-61994-FR.pdf

McCalpin, J. (1984). Preliminary age classification of landslides for inventory mapping. *Presented at the Proceedings 21st annual Engineering Geology and Soils Engineering Symposium, University Press Moscow, Idaho* (pp. 5–6).

McGuire, W. J. (1996). Volcano instability: A review of contemporary themes. *Geological Society, London, Special Publications*, *110*(1), 1–23. https://doi.org/10.1144/GSL.SP.1996.110.01.01

Merle, O., Michon, L., & Bachèlery, P. (2008). Caldera rim collapse: A hidden volcanic hazard. *Journal of Volcanology and Geothermal Research*, *177*(2), 525–530. https://doi.org/10.1016/j.jvolgeores.2008.06.011

Michon, L. (2017). *Cirque de Salazie* (pp. 1–6). Universite de la Réunion.

Migoń, P., Pánek, T., Malik, I., Hrádecký, J., Owczarek, P., & Šilhán, K. (2010). Complex landslide terrain in the Kamienne Mountains, middle Sudetes, SW Poland. *Geomorphology*, *124*(3–4), 200–214. https://doi.org/10.1016/j.geomorph.2010.09.024

Moon, V., Bradshaw, J., Smith, R., & de Lange, W. (2005). Geotechnical characterisation of stratocone crater wall sequences, White Island Volcano, New Zealand. *Engineering Geology*, *81*(2), 146–178. https://doi.org/10.1016/j.enggeo.2005.07.014

Moore, J. G., Clague, D. A., Holcomb, R. T., Lipman, P. W., Normark, W. R., & Torresan, M. E. (1989). Prodigious submarine landslides on the Hawaiian Ridge. *Journal of Geophysical Research*, *94*(B12), 17465. https://doi.org/10.1029/JB094iB12p17465

Moulin, M., & Lebon, D. (2002). *Synthèse hydrogéologique du cirque de Salazie (Ile de la réunion)* (No. RP-51127-FR) (p. 75). BRGM. Retrieved from http://infoterre.brgm.fr/rapports/RP-51127-FR.pdf

Nakazato, H., & Konishi, N. (2005). Subsurface structure exploration of wide landslide area by Aerial electromagnetic exploration. *Landslides*, *2*(2), 165–169. https://doi.org/10.1007/s10346-005-0056-2

Nichol, J. E., Shaker, A., & Wong, M.-S. (2006). Application of high-resolution stereo satellite images to detailed landslide hazard assessment. *Geomorphology*, *76*(1–2), 68–75. https://doi.org/10.1016/j.geomorph.2005.10.001

Oehler, J.-F., Labazuy, P., & Lénat, J.-F. (2004). Recurrence of major flank landslides during the last 2-Ma-history of La Réunion Island. *Bulletin of Volcanology*, *66*(7), 585–598. https://doi.org/10.1007/s00445-004-0341-2

Oehler, J.-F., Lénat, J.-F., & Labazuy, P. (2008). Growth and collapse of the La Réunion Island volcanoes. *Bulletin of Volcanology*, *70*(6), 717–742. https://doi.org/10.1007/s00445-007-0163-0

Oehler, J.-F., van Wyk de Vries, B., & Labazuy, P. (2005). Landslides and spreading of oceanic hot-spot and arc shield volcanoes on low strength layers (LSLs): An analogue modeling approach. *Journal of Volcanology and Geothermal Research*, *144*(1–4), 169–189. https://doi.org/10.1016/j.jvolgeores.2004.11.023

Okubo, C. H. (2004). Rock mass strength and slope stability of the Hilina slump, Kīlauea volcano, Hawai'i. *Journal of Volcanology and Geothermal Research*, *138*(1), 43–76. https://doi.org/10.1016/j.jvolgeores.2004.06.006

Parise, M., & Guzzi, R. (1992). *Volume and shape of the active and inactive parts of the Slumgullion Landslide, Hinsdale County, Colorado* (No 92-216, p. 32). US Department of the Interior, US Geological Survey. Retrieved from https://pubs.usgs.gov/of/1992/0216/report.pdf

Perinotto, H. (2014). Dynamique de mise en place des avalanches de débris sur les flancs aériens des volcans insulaires : le cas de La Réunion. Sciences de la Terre. Université de Bordeaux. Français. Retrieved from https://tel.archives-ouvertes.fr/tel-01147436

Perinotto, H., Schneider, J., Bachèlery, P., Le Bourdonnec, F., Famin, V., & Michon, L. (2015). The extreme mobility of Debris Avalanches: A new model of transport mechanism. *Journal of Geophysical Research: Solid Earth*, *120*(12), 8110–8119. https://doi.org/10.1002/2015JB011994

Pinchinot, H. (1984). Etude geologique des formations superficielles et du proche substratum à Grand Ilet (cirque de Salazie - La Réunion) application a la cartographie du risque de mouvements de versants. Géologie appliquée. Université Scientifique et Médicale de Grenoble. Français. Retrieved from https://tel.archives-ouvertes.fr/tel-00679334v2

Pohl, B., Morel, B., Barthe, C., & Bousquet, O. (2016). Regionalizing rainfall at very high resolution over La Réunion Island: A case study for tropical Cyclone Ando. *Monthly Weather Review*, *144*(11), 4081–4099. https://doi.org/10.1175/MWR-D-15-0404.1

Prokešová, R., Kardoš, M., & Medveďová, A. (2010). Landslide dynamics from high-resolution aerial photographs: A case study from the Western Carpathians, Slovakia. *Geomorphology*, *115*(1), 90–101. https://doi.org/10.1016/j.geomorph.2009.09.033

Quetelard, H., Bessemoulin, P., Cerveny, R. S., Peterson, T. C., Burton, A., & Boodhoo, Y. (2009). Extreme weather: World-record rainfalls during tropical Cyclone Gamede. *Bulletin of the American Meteorological Society*, *90*(5), 603–608. https://doi.org/10.1175/2008BAMS2660.1

Rault, C., Dewez, T. J. B., & Aunay, B. (2020). Structure from motion processing of aerial archive photographs: Sensitivity analyses pave the way for quantifying geomorphological changes since 1978 in La Réunion Island. *ISPRS Annals of Photogrammetry, Remote Sensing and Spatial Information Sciences, V-2–2020* (pp. 773–780). https://doi.org/10.5194/isprs-annals-V-2-2020-773-2020

Rault, C., Reninger, P. A., Samyn, K., Britri, A., Delatre, M., Thiery, Y., & Aunay, B. (2021). New insights from a multi-method geophysical investigation on a very large, slow-moving landslide (Hell Bourg, Reunion Island). *First Break*, *39*(8), 71–78. https://doi.org/10.3997/1365-2397.fb2021063

Rault, C., Thiery, Y., Aunay, B., Colas, B., Reboul, K., & Dewez, T. J. B. (2022). How can the morphometric characteristics and failure conditions of a historic gully caused by intense rainfall Be reconstructed? *Earth*, *3*(1), 324–344. https://doi.org/10.3390/earth3010020

Réchou, A., Flores, O., Jumaux, G., Duflot, V., Pouppeville, C., & Bonnardot, F. (2019). Spatio-temporal variability of rainfall in a high tropical island: Patterns and large-scale drivers in Réunion Island. *Quarterly Journal of the Royal Meteorological Society*, *145*(720), 893–909. https://doi.org/10.1002/qj.3485

Reiche, P. (1937). The Toreva-Block: A distinctive landslide type. *The Journal of Geology*, *45*(5), 538–548. https://doi.org/10.1086/624563

Remaître, A. (2006). Morphologie et dynamique des laves torrentielles : Applications aux torrents des Terres Noires du bassin de Barcelonnette (Alpes du Sud). Géomorphologie. Université de Caen. Français. Retrieved from https://tel.archives-ouvertes.fr/tel-00119737v2

Reninger, P. A., Martelet, G., Deparis, J., Perrin, J., & Chen, Y. (2011). Singular value decomposition as a denoising tool for airborne time domain electromagnetic data. *Journal of Applied Geophysics*, *75*(2), 264–276. https://doi.org/10.1016/j.jappgeo.2011.06.034

Reninger, P. A., Martelet, G., Perrin, J., & Dumont, M. (2020). Processing methodology for regional AEM surveys and local implications. *Exploration Geophysics*, *51*(1), 143–154. https://doi.org/10.1080/08123985.2019.1680249

Riquelme, A., Del Soldato, M., Tomás, R., Cano, M., Jordá Bordehore, L., & Moretti, S. (2019). Digital landform reconstruction using old and recent open access digital aerial photos. *Geomorphology*, *329*, 206–223. https://doi.org/10.1016/j.geomorph.2019.01.003

Riquier, J. (1954). Étude sur les "lavaka". Mémoires de l'Institut Scientifique de Madagascar. *Série D: Sciences de la Terre*, *6*, 169–189.

Rodrigues, D., & Ayala-Carcedo, F. (2002). Slides in Madeira Island. *Presented at the ISRM International Symposium – EUROCK 2002*.

Rossignol, C., Hallot, E., Bourquin, S., Poujol, M., Jolivet, M., Pellenard, P., et al. (2019). Using volcaniclastic rocks to constrain sedimentation ages: To what extent are volcanism and sedimentation synchronous? *Sedimentary Geology*, *381*, 46–64. https://doi.org/10.1016/j.sedgeo.2018.12.010

Roverato, M., Cronin, S., Procter, J., & Capra, L. (2015). Textural features as indicators of debris avalanche transport and emplacement, Taranaki volcano. *The Geological Society of America Bulletin*, *127*(1–2), 3–18. https://doi.org/10.1130/B30946.1

Roverato, M., Di Traglia, F., Procter, J., Paguican, E., & Dufresne, A. (2021). Factors contributing to volcano lateral collapse. In M. Roverato, A. Dufresne, & J. Procter (Eds.), *Volcanic Debris Avalanches: From collapse to hazard* (pp. 91–119). Springer International Publishing. https://doi.org/10.1007/978-3-030-57411-6_5

Salvany, T., Lahitte, P., Nativel, P., & Gillot, P. Y. (2012). Geomorphic evolution of the Piton des Neiges volcano (Réunion Island, Indian Ocean): Competition between volcanic construction and erosion since 1.4Ma. *Geomorphology*, *136*(1), 132–147. https://doi.org/10.1016/j.geomorph.2011.06.009

Samia, J., Temme, A., Bregt, A., Wallinga, J., Guzzetti, F., Ardizzone, F., & Rossi, M. (2017). Do landslides follow landslides? Insights in path dependency from a multi-temporal landslide inventory. *Landslides*, *14*(2), 547–558. https://doi.org/10.1007/s10346-016-0739-x

Schaefer, L. N., Di Traglia, F., Chaussard, E., Lu, Z., Nolesini, T., & Casagli, N. (2019). Monitoring volcano slope instability with synthetic Aperture Radar: A review and new data from Pacaya (Guatemala) and Stromboli (Italy) volcanoes. *Earth-Science Reviews*, *192*, 236–257. https://doi.org/10.1016/j.earscirev.2019.03.009

Scott, K. M., Macias, J. L., Naranjo, J. A., Rodriguez, S., & McGeehin, J. P. (2001). *Catastrophic debris flows transformed from landslides in volcanic terrains: Mobility, hazard assessment, and mitigation strategies* (No. 1630). US Department of the Interior, US Geological Survey. Retrieved from https://pubs.er.usgs.gov/publication/pp1630

Selva, J., Acocella, V., Bisson, M., Caliro, S., Costa, A., Della Seta, M., et al. (2019). Multiple natural hazards at volcanic islands: A review for the Ischia volcano (Italy). *Journal of Applied Volcanology*, *8*(1), 5. https://doi.org/10.1186/s13617-019-0086-4

Shuzui, H. (2001). Process of slip-surface development and formation of slip-surface clay in landslides in Tertiary volcanic rocks, Japan. *Engineering Geology*, *61*(4), 199–220. https://doi.org/10.1016/S0013-7952(01)00025-4

Sibrant, A. L. R., Hildenbrand, A., Marques, F. O., Weiss, B., Boulesteix, T., Hübscher, C., et al. (2015). Morpho-structural evolution of a volcanic island developed inside an active oceanic rift: S. Miguel Island (Terceira Rift, Azores). *Journal of Volcanology and Geothermal Research*, *301*, 90–106. https://doi.org/10.1016/j.jvolgeores.2015.04.011

Silva, R., Marques, R., & Gaspar, J. (2018). Implications of landslide typology and predisposing factor combinations for probabilistic landslide susceptibility models: A case study in Lajedo Parish (Flores Island, Azores—Portugal). *Geosciences*, *8*(5), 153. https://doi.org/10.3390/geosciences8050153

Smith, G. A., & Lowe, D. R. (1991). Lahars: Volcano hydrologic-events and deposition in the debris flow—Hyperconcentrated flow continuum. *Society of Sedimentary Geology (SEPM)*, *45*, 59–70. https://doi.org/10.2110/pec.91.45.0059

Sørensen, K. I., & Auken, E. (2004). SkyTEM-A new high-resolution helicopter transient electromagnetic system. *Exploration Geophysics*, *35*(3), 191–199. https://doi.org/10.1071/EG04194

Stollsteiner, P., Aunay, B., De La Torre, Y., & Delpont, G. (2008). Etude hydrogéomorphologique de la Rivière du Mât et propositions de solutions de gestion. (No. BRGM/RP-56364-FR). BRGM. Retrieved from http://ficheinfoterre.brgm.fr/document/RP-56364-FR

Stumpf, A., Malet, J.-P., Allemand, P., Pierrot-Deseilligny, M., & Skupinski, G. (2015). Ground-based multi-view photogrammetry for the monitoring of landslide deformation and erosion. *Geomorphology*, *231*, 130–145. https://doi.org/10.1016/j.geomorph.2014.10.039

Suthren, R. J. (1985). Facies analysis of volcaniclastic sediments: A review. *Geological Society, London, Special Publications*, *18*(1), 123–146. https://doi.org/10.1144/gsl.sp.1985.018.01.07

Swanson, F. J., & Swanston, D. N. (1977). Complex mass-movement terrains in the western Cascade range, Oregon. In *Reviews in engineering geology* (Vol. 3, pp. 113–124). Geological Society of America. https://doi.org/10.1130/REG3-p113

Tanyaş, H., van Westen, C. J., Allstadt, K. E., Anna Nowicki Jessee, M., Görüm, T., Jibson, R. W., et al. (2017). Presentation and analysis of a worldwide database of earthquake-induced landslide inventories. *Journal of Geophysical Research: Earth Surface*, *122*(10), 1991–2015. https://doi.org/10.1002/2017JF004236

Thiery, Y., Reninger, P. A., Lacquement, F., Raingeard, A., Lombard, M., & Nachbaur, A. (2017). Analysis of slope sensitivity to landslides by a Transdisciplinary approach in the framework of future development: The case of La Trinité in Martinique (French West Indies). *Geosciences*, *7*(4), 135. https://doi.org/10.3390/geosciences7040135

Thiery, Y., Reninger, P.-A., & Nachbaur, A. (2021). Airborne electromagnetics to improve landslide knowledge in tropical volcanic environments. *Applied Sciences*, *11*(8), 3390. https://doi.org/10.3390/app11083390

Thompson, N., Bennett, M. R., & Petford, N. (2010). Development of characteristic volcanic debris avalanche deposit structures: New insight from distinct element simulations. *Journal of Volcanology and Geothermal Research*, *192*(3–4), 191–200. https://doi.org/10.1016/j.jvolgeores.2010.02.021

Thouret, J.-C. (1999). Volcanic geomorphology—An overview. *Earth-Science Reviews*, *47*(1–2), 95–131. https://doi.org/10.1016/S0012-8252(99)00014-8

Tibaldi, A., Corazzato, C., Kozhurin, A., Lagmay, A. F. M., Pasquarè, F. A., Ponomareva, V. V., et al. (2008). Influence of substrate tectonic heritage on the evolution of composite volcanoes: Predicting sites of flank eruption, lateral collapse, and erosion. *Global and Planetary Change*, *61*(3–4), 151–174. https://doi.org/10.1016/j.gloplacha.2007.08.014

Tommasi, P., Baldi, P., Chiocci, F. L., Coltelli, M., Marsella, M., Pompilio, M., & Romagnoli, C. (2005). The landslide sequence induced by the 2002 eruption at Stromboli volcano. In K. Sassa, H. Fukuoka, F. Wang, & G. Wang (Eds.), *Landslides: Risk analysis and sustainable disaster management* (pp. 251–258). Springer. https://doi.org/10.1007/3-540-28680-2_32

Turner, A. K., & Schuster, R. L. (1996). *Landslides: Investigation and Mitigation* (Vol. 247). National Research Council.

Valadão, P., Gaspar, J. L., Queiroz, G., & Ferreira, T. (2002). Landslides density map of S. Miguel Island, Azores archipelago. *Natural Hazards and Earth System Sciences*, *2*(1/2), 51–56. https://doi.org/10.5194/nhess-2-51-2002

Vallance, J. W., & Scott, K. M. (1997). The Osceola Mudflow from Mount Rainier: Sedimentology and hazard implications of a huge clay-rich debris flow. *The Geological Society of America Bulletin*, *109*(2), 143–163. https://doi.org/10.1130/0016-7606(1997)109⟨0143:TOMFMR⟩2.3.CO;2

Van Westen, C. J., Castellanos, E., & Kuriakose, S. L. (2008). Spatial data for landslide susceptibility, hazard, and vulnerability assessment: An overview. *Engineering Geology*, *102*(3–4), 112–131. https://doi.org/10.1016/j.enggeo.2008.03.010

Van Wyk de Vries, B., & Davies, T. (2015). Landslides, Debris Avalanches, and volcanic gravitational deformation. In *The encyclopedia of volcanoes* (pp. 665–685). Elsevier. https://doi.org/10.1016/B978-0-12-385938-9.00038-9

Viezzoli, A., Christiansen, A. V., Auken, E., & Sørensen, K. (2008). Quasi-3D modeling of airborne TEM data by spatially constrained inversion. *Geophysics*, *73*(3), F105–F113. https://doi.org/10.1190/1.2895521

Vittecoq, B., Reninger, P.-A., Lacquement, F., Martelet, G., & Violette, S. (2019). Hydrogeological conceptual model of andesitic watersheds revealed by high-resolution heliborne geophysics. *Hydrology and Earth System Sciences*, *23*(5), 2321–2338. https://doi.org/10.5194/hess-23-2321-2019

Voight, B., & Elsworth, D. (1997). Failure of volcano slopes. *Géotechnique*, *47*(1), 1–31. https://doi.org/10.1680/geot.1997.47.1.1

Voight, B., Janda, R. J., Glicken, H., & Douglass, P. M. (1983). Nature and mechanics of the Mount St Helens rockslide-avalanche of 18 May 1980. *Géotechnique*, *33*(3), 243–273. https://doi.org/10.1680/geot.1983.33.3.243

Watt, S., Talling, P., & Hunt, J. (2014). New insights into the emplacement dynamics of volcanic Island landslides. *Oceanography*, *27*(2), 46–57. https://doi.org/10.5670/oceanog.2014.39

Wieczorek, G. F. (1984). Preparing a detailed landslide-inventory map for hazard evaluation and reduction. *Bulletin of the Association of Engineering Geologists*, *21*(3), 337–342. https://doi.org/10.2113/gseegeosci.xxi.3.337

Zanchetta, G., Sulpizio, R., & Di Vito, M. A. (2004). The role of volcanic activity and climate in alluvial fan growth at volcanic areas: An example from southern Campania (Italy). *Sedimentary Geology*, *168*(3), 249–280. https://doi.org/10.1016/j.sedgeo.2004.04.001

Zernack, A. V. (2021). Volcanic Debris-Avalanche Deposits in the context of volcaniclastic ring plain successions—A case study from Mt. Taranaki. In M. Roverato, A. Dufresne, & J. Procter (Eds.), *Volcanic Debris Avalanches: From collapse to hazard* (pp. 211–254). Springer International Publishing. https://doi.org/10.1007/978-3-030-57411-6_9

Zernack, A. V., & Procter, J. N. (2021). Cyclic growth and destruction of volcanoes. In M. Roverato, A. Dufresne, & J. Procter (Eds.), *Volcanic Debris Avalanches: From collapse to hazard* (pp. 311–355). Springer International Publishing. https://doi.org/10.1007/978-3-030-57411-6_12